Chapter

An In-Depth Analysis of Sliding Mode Control and Its Application to Robotics

İhsan Ömür Bucak

Abstract

In this study, a sliding mode control scheme with a bounded region and its convergence analysis are explained to the finest detail and are applied to robotic manipulators which represent the best examples for strongly coupled, highly nonlinear, time-varying dynamical systems. Simulation studies have been applied separately to two different control systems in order to demonstrate the feasibility, performance, and effectiveness of the proposed control methodology through the design of the sliding mode controller: firstly, the position control of an armature-controlled dc servo motor subject to a varying external disturbance, and secondly, a two-link robot manipulator that were also analyzed in terms of its robustness by adding extra mass to one of the joints to be able to maintain the trajectory in the sliding surface. Simulations show that a fast convergence rate, and therefore quick response, the ability to reject the varying external disturbances, and the robustness against the model uncertainty assumed to be unbounded and fast-varying have all achieved its purpose entirely. This study also examines the advantages of SMC and PID comparably. The results given here do not contradict the view that one can use it instead of the other without losing too much performance, and confirm the success of the presented approach.

Keywords: robotic manipulators, sliding mode control, convergence analysis, trajectory tracking, robustness, two-link planar robot manipulator, PID control

1. Introduction

Unknown plant parameters or, more generally, plant uncertainty and the preferences in which the system dynamics are purposely represented by simplifications, such as the use of linearized friction model, lead to model imprecision [1]. Control engineering classifies the model inaccuracies, which were used here as synonym of imprecision, into two main categories as structured and unstructured uncertainties. The first one implies inaccuracies within the model and the second one corresponds to inaccuracies on the system order (i.e., underestimated system order). Modeling inaccuracies can have adverse effect on nonlinear control systems [1].

Robotic manipulators represent the best examples for strongly coupled, highly nonlinear, time-varying dynamical systems [2]. These qualities alongside structured uncertainties caused by model imprecision of link parameters and payload variation, and unstructured uncertainties produced by unmodeled dynamics such as

nonlinear friction, compliance in gearing, sensor noise, external disturbances, and the high-frequency part of the dynamics turn the motion control of rigid-link manipulators into a complex problem [2]. Particularly, robotic manipulators suffer so much from these structured and unstructured uncertainties. The consequence of having to deal with various uncertainties in their dynamics and the necessity to manage the various tools and, hence, the variation of dynamic parameters during operation make it difficult for robots to introduce a mathematical model suitable for employing model-based control strategies.

The theory of conventional sliding mode control (SMC) as a simple robust nonlinear control scheme has been applied to robotic manipulators successfully since the 1980s. In those studies, the advantages of the SMC properties such as its robustness against disturbances and variation of parameters, and its fast dynamic response have been utilized greatly. Two important approaches, such as robust control and adaptive control, can deal with modeling uncertainty [1]. Particularly, adaptive control is effective in solving the structured and unstructured uncertainties and is capable of maintaining a uniformly good performance over a limited range.

SMC as a special class of the variable structure systems (VSS) has been preferred in practical applications for over 50 years due to its simplicity and robustness against parameter variations and disturbances [3]. VSS concept was first evolved from the pioneering work of Emel'yanov and Barbashin in the early 1960s in Russia [4]. Especially, VSS and SMC have received a great attention by the control research community worldwide since the published 1977 article [4]. SMC methodology is used to design a control law that imposes all system trajectories to converge on a surface in the state space, the so-called sliding surface $S(t)$. The designer chooses the dynamics of this surface so that all trajectories will asymptotically converge to the set point. When the trajectory lies inside the sliding surface, the system operates in so-called sliding mode and is sensitive to parametric variations and external disturbances [5]. Control action in sliding mode is discontinuous by nature and can stimulate high-frequency dynamics [6]. Discontinuous nature of the control action serves to maintain a resulting superior system performance of VSS and SMC by switching between two incomparably different system structures such that sliding mode with this feature is also referred to as a new type of system motion in a manifold, or in another substantial terms, in the vicinity of a prescribed switching manifold, the velocity vector of the controlled state trajectories is always directed toward the switching manifold by such motion induced by imposing discontinuous control actions [3, 6]. This system performance is expected to exhibit insensitivity to parameter variations as well as demonstrate complete disturbance rejection [6].

Despite its advantages such as simplicity and robustness, SMC suffers from a rather widespread and well-known chattering problem, which is generally perceived as motion oscillating about the predefined switching manifold(s) [3, 6]. There are two reasons behind the chattering phenomenon: first, under the absence of switching nonidealities such as delays, that is, in a situation where the switching device ideally switches at an infinite frequency, the presence of parasitic dynamics in series with the plant causes a small amplitude high-frequency oscillation to occur around the sliding manifold. If the closed loop pole locations are well defined or the closed loop poles are well assigned with the aid of the pole placement design technique, these parasitic dynamics which represent the fast actuator and sensor dynamics are often neglected in the open loop model used for control design in control applications. In general, the motion of the real system is closer to an ideal system where the parasitic dynamics are neglected, and the difference between the ideal and the real motion, which is at negligible time constants, shows a rapid decline. However, the parasitic dynamics interacted with variable structure control

(VSC) in particular produce a nondecreasing oscillatory component with a finite amplitude and a frequency, referred previously to as chattering phenomenon already. Second, the switching nonidealities alone can cause such high-frequency oscillations around the sliding surface $S(t)$ [3, 6]. These may include small time delays due to sampling (e.g., zero-order hold), execution time required to calculate the control, and transmission delays in networked control systems [3]. As time delays cause the resulting chattering phenomenon, and the delay type of switching nonidealities is the most relevant to any electronic implementation of the switching device whether it includes analogue or digital circuits, delay type nonidealities are considered in general for the design approaches, and discrete-time control design techniques are the most commonly used design approaches by control engineers to mitigate the chattering caused by the switching delays [6]. Many design methodologies have been applied so far to mitigate or reduce the chattering. To eliminate the chattering, a boundary layer around the sliding surface $S(t)$ has been introduced [1]. Inside the boundary layer, the switching function is replaced by a high-gain proportional control [5]. In order to reduce the chattering level, several switching functions such as saturation functions, relay functions, hyperbolic functions, and hysteresis saturation functions have been used in literature. The use of these functions can minimize or, if desired, completely eliminate the chattering, but it turns perfect tracking into a tracking with a guaranteed precision problem, meaning that a steady-state error is always maintained.

SMC design procedure is split into two major steps corresponding to the two main phases [3]: reaching phase is defined to derive the system state from initial state to reach the switching manifolds in finite time; and sliding-mode phase is defined to induce the system into the sliding motion on the switching manifolds like an attractor.

No matter how active the research on SMC has been during the last 50 years, the key technical challenges such as chattering, the elimination of the effects caused by unmodeled dynamics, disturbances and uncertainties, adaptive learning, and improved robustness can still remain to be addressed to reach a perfect solution [3]. An ideal sliding mode can only be achieved when the dynamic equation governing the sliding mode is satisfied by the system state for all time. This implies an infinite switching to assure the sliding motion [3]. Although the switching rate of the switching control device of the SMC system (design) is infinite ideally, it is much lower than that in practice due to the physical limitations of switching [6]. Physical limitations of switching have been tried to be explained in the previous paragraphs.

Usually, intelligent control approaches can mitigate the effects of structured parametric uncertainty and unstructured disturbance with their effective learning ability without requiring a detailed knowledge of the controlled plant within the design process. SMC research has recently been integrated with intelligent control approaches such as neural networks, fuzzy logic, genetic algorithms, and probabilistic reasoning, just a few of them, to make it more intelligent [3, 7–11]. Another goal behind the combination of the intelligent control with the attractive features of this traditional control is to create more powerful control algorithms. Nevertheless, it appears that many intelligent control algorithms do not take into account actuator dynamics in robot control systems, which play a critical role in overall robot dynamics and their negligence can cause adverse effects, especially in the case of high-speed torque, respectable load variations, friction, and actuator saturations [2]. Electrical actuators are very much controllable than others and are more suitable for driving robot manipulators [2, 12].

Sliding mode control strategy is the simple approach to robust control. By intuition, controlling first-order systems is much easier than controlling general *nth*-order systems, even if they are nonlinear or uncertain. Therefore, an introduction of

a notational simplification allows *nth*-order problems to be replaced by equivalent first-order problems. Thus, it is then easy to demonstrate in principle the achievement of perfect performance under the presence of arbitrary parameter inaccuracies for the transformed problems. However, such performance is only achieved at the expense of extremely high control activity. This is typically disputed by the other source of modeling uncertainty, such as the presence of neglected dynamics, which the high control activity can stimulate. This leads to a change in control laws aimed at achieving an effective trade-off between tracking performance and parametric uncertainty, given the acceptable control activity [1].

The concepts will first be presented for systems that have a single control input that allows us to develop an intuition about the fundamental aspects of nonlinear controller design.

2. Sliding surfaces

Consider the single-input dynamic system given below:

$$x^{(n)} = f(\boldsymbol{x}) + b(\boldsymbol{x})u, \tag{1}$$

where the scalar x is the output we are interested in, the scalar u is called the control input, and $\boldsymbol{x} = \left[x, \dot{x}, \ldots, x^{(n-1)}\right]^T$ represents the state vector. While the function $f(\boldsymbol{x})$ in (1) is not exactly known, an upper bound on $f(\boldsymbol{x})$ is set by a known continuous function of $\boldsymbol{x}$ to limit the size of the imprecision. Similarly, the control gain $b(\boldsymbol{x})$ is not exactly known either, only its sign is known; therefore, it is also bounded by the known continuous functions of $\boldsymbol{x}$. The control problem is to ensure that the state $\boldsymbol{x}$ tracks an explicit time-varying state $\boldsymbol{x}_d = \left[x_d, \dot{x}_d, \ldots, {x_d}^{(n-1)}\right]^T$ in the presence of model imprecision on $f(\boldsymbol{x})$ and $b(\boldsymbol{x})$. In order for the tracking task to be achieved using a finite control u, desired initial state $\boldsymbol{x}_d(0)$ must be such that it ultimately validates the following relationship:

$$\boldsymbol{x}_d(0) = \boldsymbol{x}(0) \tag{2}$$

For example, in a second-order system, the position or speed cannot bounce; as a result of this fact, any desired trajectory that can be workable from time $t = 0$ necessarily starts at the same position and speed as those of the plant.

2.1 A notational simplification

Let us define $\tilde{x} = x - x_d$ as the tracking error in the variable x, and $\tilde{\boldsymbol{x}} = \boldsymbol{x} - \boldsymbol{x}_d = \left[\tilde{x}, \dot{\tilde{x}}, \ldots, \tilde{x}^{(n-1)}\right]^T$ as the tracking error vector. Let us also define a surface $S(t)$ that is time-varying in the state-space $\boldsymbol{R}^{(n)}$ with the scalar equation $s(\boldsymbol{x}; t) = 0$ expressed as:

$$s(\boldsymbol{x}; t) = \left(\frac{d}{dt} + \lambda\right)^{n-1} \tilde{x}, \tag{3}$$

where λ is a strictly positive constant. For example, if $n = 2$, Eq. (3) takes the following form:

$$s = \dot{\tilde{x}} + \lambda \tilde{x},$$

that is, it simply consists of a weighted sum of the position and the velocity errors; thus, we can express $\tilde{x}$ from Eq. (3) as follows:

$$\tilde{x} = \frac{s(\boldsymbol{x}; t)}{\left(\frac{d}{dt} + \lambda\right)^{n-1}} \tag{4}$$

More specifically, a first-order stabilization problem in s is basically nothing other than a replacement for the problem of tracking the n-dimensional vector $\boldsymbol{x}_d$ (i.e., the original *nth*-order tracking problem in x). Indeed, s needs to be differentiated only once for the appearance of the input u due to the presence of the term $\tilde{x}^{(n-1)}$ in the expression s in (3).

Additionally, the bounds on s can be evaluated directly as the bounds on the tracking error vector $\tilde{\boldsymbol{x}}$, and therefore, the scalar s is considered a true measure of tracking performance. Specifically, under the assumption that $\tilde{\boldsymbol{x}}(0) = \boldsymbol{0}$ (in the meantime, we make a note that the effect of non-zero initial conditions in $\tilde{x}$ can be added separately), we write:

$$\forall t \geq 0, |s(t)| \leq \Phi \Rightarrow \forall t \geq 0, \left|\tilde{x}^{(i)}(t)\right| \leq (2\lambda)^i \varepsilon \qquad i = 0, \ldots, n-1 \tag{5}$$

where $\varepsilon = \Phi/\lambda^{n-1}$. Indeed, Eq. (3), or more precisely, Eq. (4) derived from (3) clearly indicates that the tracking error $\tilde{\boldsymbol{x}}$ can be obtained from s through a sequence of first-order low-pass filters (see **Figure 1**, where $p = (d/dt)$ is commonly known as the *Laplace operator*).

In general, a first-order low-pass filter's input-output relationship is given as follows:

$$\frac{Output_{lpf}}{Input_{lpf}} = K_f \frac{1}{1 + p\tau},$$

where K_f is filter gain and τ is filter time constant. Let y_1 be the output of the first filter. We can express the output of the first filter in terms of a *convolution integral* in time domain by taking into account the fact that the input is already defined as s:

$$y_1(t) = \int_0^t e^{-\lambda(t-T)} s(T) dT.$$

Using $|s| \leq \Phi$, we get the following:

$$\left|y_1(t)\right| \leq \Phi \int_0^t e^{-\lambda(t-T)} dT = \frac{\Phi}{\lambda} e^{-\lambda(t-T)}\Big]_0^t = \frac{\Phi}{\lambda}\left(1 - e^{-\lambda t}\right) \leq \Phi/\lambda.$$

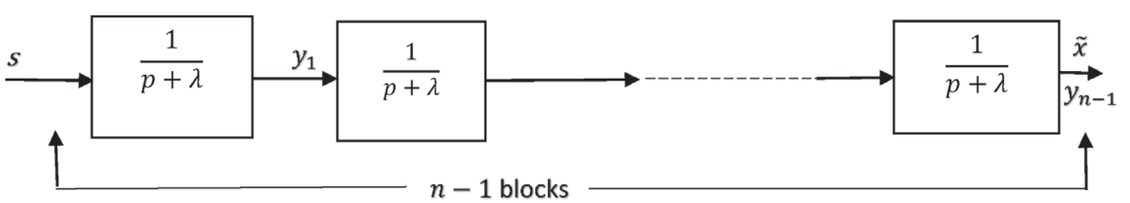

Figure 1.
Computing bounds on $\tilde{x}$.

We can apply similar reasoning to the second filter, et cetera, until we reach $y_{n-1} = \tilde{x}$. Ultimately, we get

$$|\tilde{x}| \leq \Phi/\lambda^{n-1} = \varepsilon.$$

Similarly, $\tilde{x}^{(i)}$can be considered to be acquired through the sequence of **Figure 2**.

One can easily make another similar relationship, $|z_I| \leq \Phi/\lambda^{n-1-i}$ by referring to the previous result. Here, z_I is the output of the $(n-i-1)^{th}$ filter. It is worth noting, however, that

$$\frac{p}{p+\lambda} = \frac{p+\lambda-\lambda}{p+\lambda} = 1 - \frac{\lambda}{p+\lambda}.$$

One sees that the remaining i blocks right after $n-i-1$ blocks in the sequence of **Figure 2** include numerators of p as can typically be seen in practical filter applications, and that the sequence of **Figure 2** means that

$$\left|\tilde{x}^{(i)}\right| \leq \left(\frac{\Phi}{\lambda^{n-1-i}}\right) \underbrace{\left(1 - \frac{\lambda}{p+\lambda}\right) \ldots \ldots \left(1 - \frac{\lambda}{p+\lambda}\right)}_{i \text{ blocks}},$$

where the first multiplier to the right of inequality sign includes the first $n-i-1$ blocks which do not have p as the numerator. When i blocks multipliers are arranged, the expression takes the form:

$$\left|\tilde{x}^{(i)}\right| \leq \left(\frac{\Phi}{\lambda^{n-1-i}}\right) \left(\underbrace{1 \ldots \ldots \ldots \ldots 1}_{i \text{ times}} + \frac{\lambda \ldots \ldots \lambda}{\lambda^i}\right),$$

where term comes from the result derived for the sequential blocks each of which is represented by $1/(p+\lambda)$, and $1/(p+\lambda)^i \leq 1/\lambda^i$. Besides, the positive sign must be considered to obtain the prospective upper bound. In this case, the next step is:

$$\left|\tilde{x}^{(i)}\right| \leq \left(\frac{\Phi}{\lambda^{n-1-i}}\right) \left(1^i + \frac{\lambda^i}{\lambda^i}\right).$$

Finally, we can write,

$$\left|\tilde{x}^{(i)}\right| \leq \left(\frac{\Phi}{\lambda^{n-1-i}}\right) \left(1 + \frac{\lambda}{\lambda}\right)^i$$

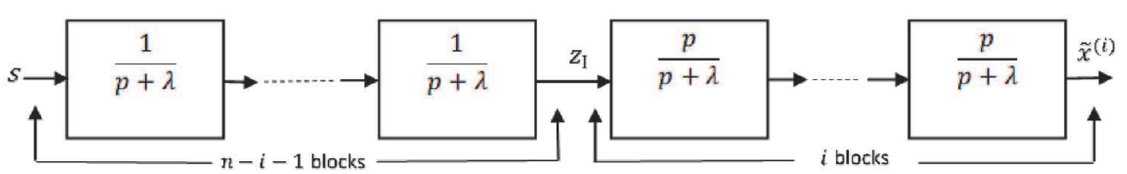

Figure 2.
Computing bounds on $\tilde{x}^{(i)}$.

since $\left(1^i + \frac{\lambda^i}{\lambda^i}\right) \leq \left(1 + \frac{\lambda}{\lambda}\right)^i$. Thus, as a result, we reach the following statement:

$$\left|\tilde{x}^{(i)}\right| \leq \left(\frac{\Phi}{\lambda^{n-1}}\right)\lambda^i(1+1)^i = \left(\frac{\Phi}{\lambda^{n-1}}\right)(2\lambda)^i = (2\lambda)^i\varepsilon,$$

i.e., the bounds of (5) are proven. Finally, in the case where $\tilde{\boldsymbol{x}}(0) \neq \mathbf{0}$, the bounds of (5) are obtained asymptotically, that is, within a short time constant $(n-1)/\lambda$. Please note that since the single filter block has a time constant equal to $1/\lambda$ as seen from the above analysis starting from (3), the sequence of $(n-1)$ filter blocks will have the time constants equal to $(n-1)/\lambda$.

Hence, we, indeed, have replaced an *nth*-order *tracking problem* by a first-order *stabilization problem*, and have quantified with inequality (5) the transformations in which the performance measures correspond to.

Keeping the scalar s at zero, which is a simplified first-order problem, can now be achieved by choosing the control law u of (1) such that apart from $S(t)$

$$\frac{1}{2}\frac{d}{dt}s^2 \leq -\eta|s|, \tag{6}$$

where η is a strictly positive design constant and ensures inequality (6) which is called η- reachability condition. A fundamental requirement is that the sliding mode dynamics must be attractive to the system state and there are many reachability conditions defined in the literature [13–17]. Basically, inequality (6) indicates that the squared "distance" to the surface, as measured by s^2, decreases throughout entire system trajectories. Therefore, it restricts trajectories to head toward the surface $S(t)$, as depicted in **Figure 3**. Particularly, when they are on the surface, the system trajectories remain on the surface. In other words, the fact that the surface is an *invariant set* indicates that condition (6) (a.k.a., *sliding condition*) is satisfied. Moreover, as we shall notice, inequality (6) also suggests tolerating some disturbances or dynamic uncertainties while still holding the surface stationary (i.e., an invariant set). In **Figure 3**, this graphically means that the trajectories away from the surface can "move" while still denoting the surface. $S(t)$ verifying (6) is referred to as a *sliding surface*, and the system behavior that occurs on the surface is called *sliding regime* or *sliding mode*.

Another appealing feature of the invariant set $S(t)$ is that when the system trajectories are on the set, it is defined by the equation of the set itself, i.e.,

$$\left(\frac{d}{dt} + \lambda\right)^{n-1}\tilde{x} = 0.$$

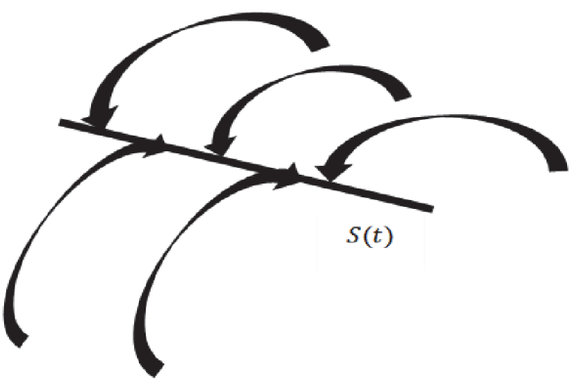

Figure 3.
The sliding condition.

That is to say, the surface $S(t)$ represents both a place and a dynamics. This fact is clearly the geometric interpretation of our previous statement that definition (3), in fact, allows us to substitute a first-order problem for an *nth*-order one.

Finally, if condition (2) is not fully validated, i.e., if $\boldsymbol{x}(t=0)$ is indeed away from $\boldsymbol{x}_d(t=0)$, then, nevertheless, satisfying (6) gives a guarantee for reaching the surface $S(t)$ at a *finite time* smaller than $|s(t=0)|/\eta$. Indeed, assume, for instance, that $s(t=0)>0$ and define t_{reach} as the time needed to hit the surface $s=0$. Integrating (6) between the points $t=0$ and $t=t_{reach}$ (i.e., in the interval $[0, t_{reach}]$) gives rise to:

$$0 - s(t=0) = s(t=t_{reach}) - s(t=0) \leq -\eta(t_{reach} - 0),$$

which means that

$$t_{reach} \leq s(t=0)/\eta. \tag{7}$$

This result can simply be proven to be true by starting to integrate both sides of (6) between 0 and t_{reach} as follows:

$$\int_{t=0}^{t=t_{reach}} \frac{1}{2}\frac{d}{dt}s^2 dt \leq -\int_{t=0}^{t=t_{reach}} \eta|s|dt.$$

Making the necessary simplifications within the integrals, we get the following:

$$\int_{t=0}^{t=t_{reach}} ds \leq -\int_{t=0}^{t=t_{reach}} \eta dt.$$

Now, the integrals are taken and evaluated for the lower and upper limits as shown below:

$$s(t=t_{reach}) - s(t=0) \leq -\eta(t_{reach} - 0).$$

Finally from here,

$$s(t=0) \geq \eta t_{reach}$$

is written, and the same result as (7) is hereby obtained. Even if $s(t=0)<0$, a similar result would be obtained, and thus, writing the above inequality as follows would be a correct representation:

$$t_{reach} \leq |s(t=0|/\eta.$$

Furthermore, definition (3) implies that once on the surface, the tracking error tends exponentially to zero, with a time constant $(n-1)/\lambda$.

The typical system behavior implied by satisfying sliding condition (6) is shown in **Figure 4** for $n=2$. A line with slope $-\lambda$ and containing the time-varying point $\boldsymbol{x}_d = [x_d \;\; \dot{x}_d]^T$ represents the sliding surface in the phase plane. The state trajectory reaches the time-varying surface in a finite time smaller than $s(t=0)/\eta$ from any initial condition, and then slides across the surface towards $\boldsymbol{x}_d$ exponentially, with a time constant equal to $1/\lambda$.

In conclusion, the idea behind (3) and (6) is to obtain an appropriate function of the tracking error, s, in accordance with (3), and then choose the feedback control law u in (1) such that s^2 continues to be used as a Lyapunov-like function of the closed-loop system, in spite of the presence of model imprecision and of

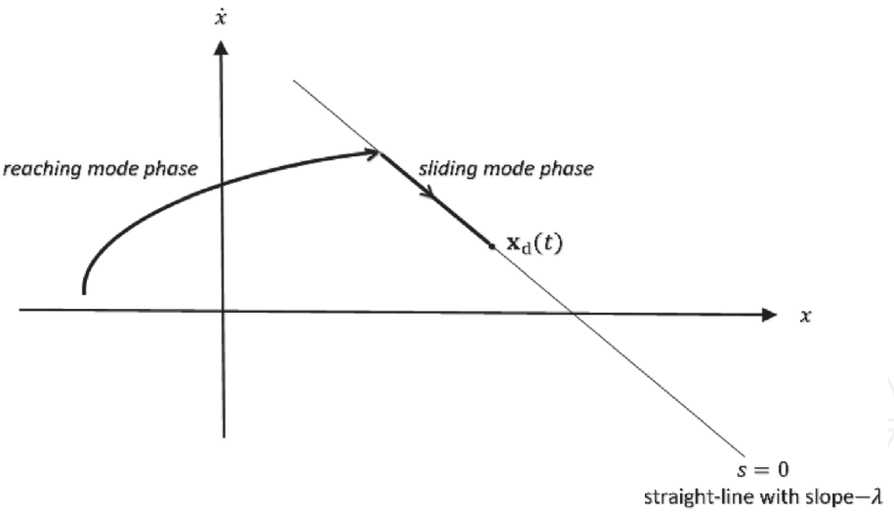

Figure 4.
Graphically represented Eqs. (3) and (6) for $n = 2$.

disturbances. Then, the controller design is a two-step procedure. First, the selection of a feedback control law u is performed to verify sliding condition (6). However, it is required that the control law be *discontinuous throughout* $S(t)$ to take into account the presence of modeling imprecision and of disturbances. Since the execution of the associated control switchings is not necessarily perfect (for instance, in practice, switching is not instantaneous, and the value of s is not known with infinite precision), this causes *chattering* (**Figure 5**). Now, with a few important exceptions, chattering is practically undesirable, because it contains high control activity and can trigger neglected high-frequency dynamics during modeling (such as unmodeled structural modes, neglected time-delays, etc.). Thus, in a second step, the *discontinuous control law* u is *smoothed accordingly to reach an optimal compromise between control bandwidth and tracking precision*: while the first step explains parametric uncertainty, the second step ensures robustness to high-frequency unmodeled dynamics.

As mentioned previously, the discontinuous control law causes chattering of the trajectories to take place around the surface $s = 0$. This problem can be eliminated

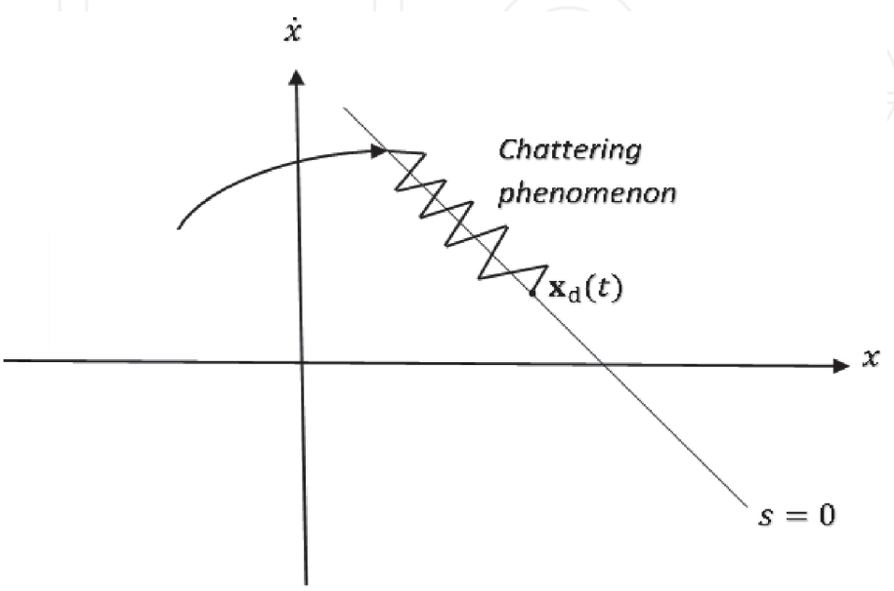

Figure 5.
Chattering caused by the switching delays.

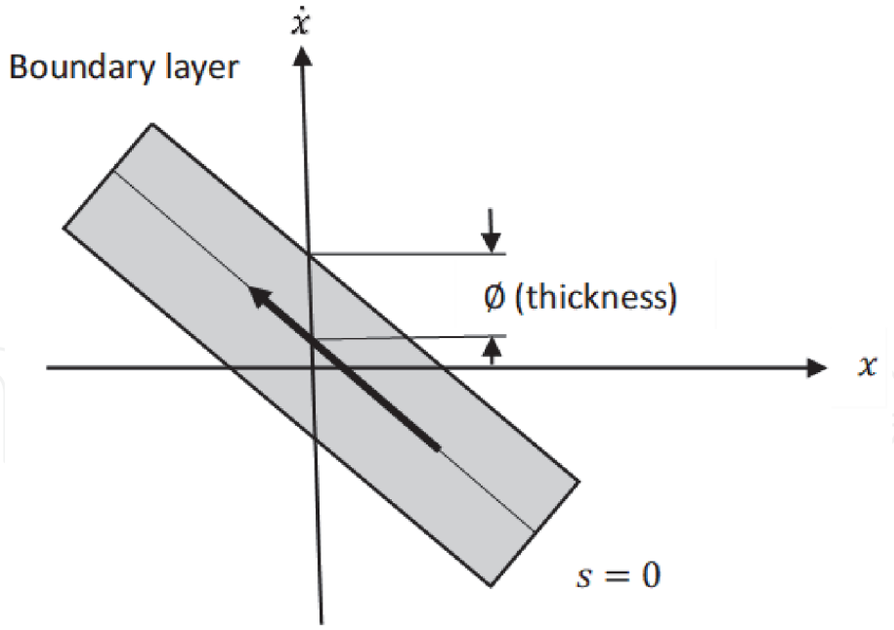

Figure 6.
Boundary layer with thickness ∅.

by smoothing out the discontinuities in the vicinity of the sliding surface through the introduction of a boundary layer thickness. An adaptation of saturation nonlinearity instead of signum nonlinearity in a position control system in which it is represented by Eqs. (83) and (84) in order to decrease the chattering phenomenon caused by sliding mode control law is the result of the same effort of smoothing out the discontinuities with the introduction of the boundary layer thickness as illustrated in **Figure 6**.

To maintain the system work in the sliding surface, a switching action term, u_{sw}, is added to the control law, and is defined by

$$u_{sw} = -Ksat(s),$$

and overall control law can be expressed as:

$$u = \hat{u} + u_{sw} = \underbrace{\left(-\hat{f} + \ddot{x}_d - \lambda\dot{\tilde{x}}\right)}_{\text{Low frequency control}} - \underbrace{Ksat(s)}_{\text{High frequency control}},$$

which will be explained in more detail in Section 5.1. Here, the nonlinear saturation function $sat(s)$, which is the replacement for nonlinear signum function $sgn\,(s)$, is defined by

$$sat(s) = \begin{cases} -1, & \frac{s}{\varnothing} < 0 \\ 0, & \left|\frac{s}{\varnothing}\right| < 1, \\ 1, & \frac{s}{\varnothing} < -1 \end{cases}$$

where ∅ is the boundary layer thickness.

3. Sliding mode control design

A continuous-time dynamical equation of an n-link robot manipulator is defined as follows:

$$\boldsymbol{M}(\boldsymbol{q})\ddot{\boldsymbol{q}} + \boldsymbol{C}(\boldsymbol{q},\dot{\boldsymbol{q}})\dot{\boldsymbol{q}} + \boldsymbol{F}(\dot{\boldsymbol{q}}) + \boldsymbol{G}(\boldsymbol{q}) = \boldsymbol{\tau}, \tag{8}$$

where $\boldsymbol{q} \in \boldsymbol{R}^{nx1}$ denotes the joint configuation variables (translational or rotational) representing the generalized position coordinates (alias the joint positions) of the robot links. Similarly, $\dot{\boldsymbol{q}}, \ddot{\boldsymbol{q}} \in \boldsymbol{R}^{nx1}$ represent the joint velocity and acceleration of the robot links, respectively. $\boldsymbol{M}(\boldsymbol{q}) \in \boldsymbol{R}^{nxn}$ is the symmetric, bounded, positive definite inertia mass matrix. $\boldsymbol{C}(\boldsymbol{q},\dot{\boldsymbol{q}}) \in \boldsymbol{R}^{nxn}$ is the matrix of Coriolis and centripetal forces and $\boldsymbol{F}(\dot{\boldsymbol{q}}) \in \boldsymbol{R}^{nx1}$ is the vector of viscous friction. Furthermore, the vector of $\boldsymbol{G}(\boldsymbol{q}) \in \boldsymbol{R}^{nx1}$ represents the gravity terms, and finally, $\boldsymbol{\tau} \in \boldsymbol{R}^{nx1}$ is called the control torque vector, or the vector of applied joint torques.

Sliding surface defined below is considered in the design of SMC controller:

$$\boldsymbol{s} = \dot{\boldsymbol{e}} + \boldsymbol{\lambda}\boldsymbol{e}, \tag{9}$$

where $\boldsymbol{e} = -\tilde{\boldsymbol{q}} = \boldsymbol{q} - \boldsymbol{q}_d$ represents the error vector and $\boldsymbol{\lambda}$ is assumed to be a symmetric positive definite matrix such that $\boldsymbol{s} = \boldsymbol{0}$ would evolve into a stable surface. The reference velocity vector $\dot{\boldsymbol{q}}_r$ is the same as the definition in [1]:

$$\dot{\boldsymbol{q}}_r = \dot{\boldsymbol{q}}_d - \boldsymbol{\lambda}\boldsymbol{e}. \tag{10}$$

Hence, one can define the sliding surface as follows:

$$\boldsymbol{s} = \dot{\boldsymbol{q}} - \dot{\boldsymbol{q}}_r. \tag{11}$$

Now, the following lemma refers to the sliding mode controller design.

Lemma 1. *Let us consider the system consisting of (8) through (10). If the following control rule is selected:*

$$\boldsymbol{\tau} = \hat{\boldsymbol{\tau}} - \boldsymbol{K}_{sg}\, sgn\,(\boldsymbol{s}) \tag{12}$$

such that

$$\hat{\boldsymbol{\tau}} = \boldsymbol{M}\ddot{\boldsymbol{q}}_r + \hat{\boldsymbol{C}}\ddot{\boldsymbol{q}}_r + \boldsymbol{G} \tag{13}$$

and

$$K_{sg_i} \geq \left\|\Delta \boldsymbol{C}\dot{\boldsymbol{q}}_r\right\| + \Gamma_i, \tag{14}$$

then the following sliding condition [1],

$$\frac{1}{2}\frac{d}{dt}\left[\boldsymbol{s}^T\boldsymbol{M}\boldsymbol{s}\right] < -\eta\left(\boldsymbol{s}^T\boldsymbol{s}\right)^{1/2}, \eta > 0 \tag{15}$$

is satisfied. In (14), K_{sg_i} stands for the element of sliding gain vector $\boldsymbol{K}_{sg}$ and $\boldsymbol{\Gamma}$ is a design parameter vector that must be chosen to ensure the inequality $\Gamma_i \geq F_{up} + \eta_i$.

Proof. Let Lyapunov function candidate be given as follows:

$$V = \frac{1}{2}\boldsymbol{s}^T\boldsymbol{M}\boldsymbol{s}. \tag{16}$$

Since $\boldsymbol{M}$ is positive definite and $\boldsymbol{s}$ is different from zero ($\boldsymbol{s} \neq \boldsymbol{0}$), V is always greater than zero ($V > 0$) and by taking time derivative of (16) and taking into account the symmetric property of $\boldsymbol{M}$, it takes the following form:

$$\dot{V} = \frac{1}{2}\dot{\boldsymbol{s}}^T\boldsymbol{M}\boldsymbol{s} + \frac{1}{2}\boldsymbol{s}^T\left(\dot{\boldsymbol{M}}\boldsymbol{s} + \boldsymbol{M}\dot{\boldsymbol{s}}\right) = \frac{1}{2}\dot{\boldsymbol{s}}^T\boldsymbol{M}\boldsymbol{s} + \frac{1}{2}\boldsymbol{s}^T\dot{\boldsymbol{M}}\boldsymbol{s} + \frac{1}{2}\boldsymbol{s}^T\dot{\boldsymbol{M}}\boldsymbol{s} = \boldsymbol{s}^T\boldsymbol{M}\dot{\boldsymbol{s}} + \frac{1}{2}\boldsymbol{s}^T\dot{\boldsymbol{M}}\boldsymbol{s} \tag{17}$$

Using (11), we get:

$$\dot{V} = \boldsymbol{s}^T\boldsymbol{M}\left(\ddot{\boldsymbol{q}} - \ddot{\boldsymbol{q}}_r\right) + \frac{1}{2}\boldsymbol{s}^T\dot{\boldsymbol{M}}\boldsymbol{s} = \boldsymbol{s}^T\left(\boldsymbol{M}\ddot{\boldsymbol{q}} - \boldsymbol{M}\ddot{\boldsymbol{q}}_r\right) + \frac{1}{2}\boldsymbol{s}^T\dot{\boldsymbol{M}}\boldsymbol{s} \tag{18}$$

Taking $\ddot{\boldsymbol{q}}$ from (8) and replacing it in (18), we have:

$$\dot{V} = \boldsymbol{s}^T\left(\boldsymbol{M}\boldsymbol{M}^{-1}\left(\boldsymbol{\tau} - \boldsymbol{C}\dot{\boldsymbol{q}} - \boldsymbol{G} - \boldsymbol{F}\right) - \boldsymbol{M}\ddot{\boldsymbol{q}}_r\right) + \frac{1}{2}\boldsymbol{s}^T\dot{\boldsymbol{M}}\boldsymbol{s}.$$

Then, taking $\dot{\boldsymbol{q}}$ from (11) and replacing it above yields:

$$\dot{V} = \boldsymbol{s}^T\left(\boldsymbol{\tau} - \boldsymbol{C}\dot{\boldsymbol{q}}_r - \boldsymbol{G} - \boldsymbol{F} - \boldsymbol{M}\ddot{\boldsymbol{q}}_r\right) + \frac{\boldsymbol{s}^T\left(\dot{\boldsymbol{M}} - 2\boldsymbol{C}\right)\boldsymbol{s}}{2}.$$

In the above equation, the second term is zero due to the *asymmetry property*; therefore, it disappears. In this new case,

$$\dot{V} = \boldsymbol{s}^T\left(\boldsymbol{\tau} - \boldsymbol{C}\dot{\boldsymbol{q}}_r - \boldsymbol{G} - \boldsymbol{F} - \boldsymbol{M}\ddot{\boldsymbol{q}}_r\right). \tag{19}$$

Next, applying (12) and (13) successively for $\boldsymbol{\tau}$ and $\hat{\boldsymbol{\tau}}$ in Eq. (19), and proceeding step by step, the following result is reached:

$$\dot{\boldsymbol{V}} = \boldsymbol{s}^T\left(\left(\hat{\boldsymbol{C}} - \boldsymbol{C}\right)\dot{\boldsymbol{q}}_r - \boldsymbol{K}_{sg}sgn(\boldsymbol{s}) - \boldsymbol{F}\right) = \boldsymbol{s}^T\left(-\Delta\boldsymbol{C}\dot{\boldsymbol{q}}_r - \boldsymbol{K}_{sg}\,sgn\,(\boldsymbol{s}) - \boldsymbol{F}\right). \tag{20}$$

In robot modeling, the terms $\boldsymbol{M}(\boldsymbol{q})$ and $\boldsymbol{G}(\boldsymbol{q})$ can be well and accurately determined, but in most cases it is not easy to have the parameters $\boldsymbol{C}(\boldsymbol{q}, \dot{\boldsymbol{q}})$ and $\boldsymbol{F}(\dot{\boldsymbol{q}})$ precisely. Therefore, in this work, the matrix $\boldsymbol{C}$ is considered

$$\boldsymbol{C} = \hat{\boldsymbol{C}} + \Delta\boldsymbol{C}, \tag{21}$$

where $C_{i,j}$ stands for the elements of the matrix $\boldsymbol{C}$. Also, the vector $\boldsymbol{F}$ is assumed an external disturbance with the upper bound defined as,

$$\|\boldsymbol{F}\| \leq F_{up}, \tag{22}$$

where the operator $\|.\|$ denotes Euclidian norm [2]. Now, by rearranging (20) as shown step by step below, we get the following:

$$\dot{V} = -\boldsymbol{s}^T\left(\Delta\boldsymbol{C}\dot{\boldsymbol{q}}_r + \boldsymbol{F}\right) - \boldsymbol{s}^T\boldsymbol{K}_{sg}\,sgn\,(\boldsymbol{s}) = -\boldsymbol{s}^T\left(\Delta\boldsymbol{C}\dot{\boldsymbol{q}}_r + \boldsymbol{F}\right) - \sum_{\boldsymbol{i}=1}^{\boldsymbol{n}} K_{sg_{\boldsymbol{i}}}|s_{\boldsymbol{i}}|, \tag{23}$$

where $|s_i| = {s_i}^T\,sgn\,(s_i)$.

At this point, we can briefly verify that the terms on the right side of (14) are positive. First of all, it is easiest to say that the first term on the right, $\left\|\Delta \boldsymbol{C}\dot{\boldsymbol{q}}_r\right\|$, is positive in any case, because the Euclidian norm is used. The other term Γ_i is also positive. Because, as we have already stated in (14) that $\Gamma_i \geq F_{up} + \eta_i$, where F_{up} is an unknown upper bound defined as $\|\boldsymbol{F}\| \leq F_{up}$ in (22), which also indicates that it is absolutely positive, and η is a strictly positive design constant and ensures inequality (6). Hence, $\Gamma_i \geq 0$. Now, if the inequality K_{sg_i} given by (14) is substituted in Eq. (23) under the acceptance of its equality sign for a moment, we can rewrite Eq. (23) by extending it as follows:

$$\dot{V} = -\boldsymbol{s}^T\left(\Delta \boldsymbol{C}\dot{\boldsymbol{q}}_r + \boldsymbol{F}\right) - \sum_{i=1}^{n}\left\|\Delta \boldsymbol{C}\dot{\boldsymbol{q}}_r\right\||s_i| - \sum_{i=1}^{n} F_{up}|s_i| - \sum_{i=1}^{n}\eta_i|s_i|.$$

The first, second and third terms on the right side of the equation above are negative in varying amounts and contribute to the final term, which is $\sum_{i=1}^{n}\eta_i|s_i|$, more negatively. Therefore, we can easily conclude that

$$\dot{V} \leq -\sum_{i=1}^{n}\eta_i|s_i|. \tag{24}$$

This shows that V is a Lyapunov function and the satisfaction of sliding condition in (15) is proven.

4. Achievement of the control law for robot manipulators for the adapted reaching mode

VSC systems include a group of different, generally fairly simple, feedback control laws and a decision rule. Depending on the system condition, a decision rule, usually called the *switching function*, determines which control law is "on-line" at any time. The transient dynamics of VSC systems consists of two modes: a "reaching mode" (or "non-sliding mode"), and a subsequent "sliding mode". Hence, VSC design involves two stages: the first one involves the design of the appropriate n-dimensional switching function $\boldsymbol{s}(\boldsymbol{x})$ for a desired sliding mode dynamics. The second one involves a control design for the reaching mode where a reaching condition is met. The desired sliding mode dynamics usually includes a fast and stable error-free response without overshoot. In sliding mode, an asymptotic convergence to the final state will be accomplished. The desired response in the reaching mode, in general, is to reach the switching manifold defined as

$$\boldsymbol{s}(\boldsymbol{x}) = \boldsymbol{\psi}^T\boldsymbol{x} = \boldsymbol{0}, \tag{25}$$

in a finite time with a small amount of overshoot with regard to the switching manifold [18].

The reaching law is a differential equation that determines the dynamics of a switching function $\boldsymbol{s}(\boldsymbol{x})$. If $\boldsymbol{s}(\boldsymbol{x})$ is an asymptotically stable differential equation, then, it is solely a reaching condition. Further, the parameter selection in the differential equation controls the dynamic quality of the VSC system in the reaching mode. The reaching law can be expressed practically in general form as follows [18]:

$$\dot{\boldsymbol{s}} = -\boldsymbol{Q}sgn(\boldsymbol{s}) - \boldsymbol{K}\boldsymbol{h}(\boldsymbol{s}), \tag{26}$$

where $\boldsymbol{Q} = diag[q_1, \ldots, q_n]$, $q_i > 0$; $sgn(\boldsymbol{s}) = [sgn(s_1), \ldots, sgn(s_n)]^T$; $\boldsymbol{K} = diag[k_1, \ldots, k_n]$, $k_i > 0$; $\boldsymbol{h}(\boldsymbol{s}) = [h_1(s_1), \ldots, h_n(s_n)]^T$; and $s_i h_i(s_i) > 0$, $h_i(0) = 0$.

The design principle of the SMC law for the plants of arbitrary order is to force a variable's error and its derivative to zero. Tracking of a desired motion $\boldsymbol{q}^d(t)$ is the main task of the robot arm. Here, let us start first by defining a $2n$-dimensional error vector [18]:

$$\boldsymbol{e} = \begin{bmatrix} \boldsymbol{e}_1 \\ \boldsymbol{e}_2 \end{bmatrix} = \begin{bmatrix} \boldsymbol{q}^d - \boldsymbol{x}_1 \\ \dot{\boldsymbol{q}}^d - \boldsymbol{x}_2 \end{bmatrix} = \begin{bmatrix} \boldsymbol{q}^d - \boldsymbol{q} \\ \dot{\boldsymbol{q}}^d - \dot{\boldsymbol{q}} \end{bmatrix}, \tag{27}$$

and then, an n-dimensional vector of switching function:

$$\boldsymbol{s}(\boldsymbol{e}) = \boldsymbol{\Psi}\boldsymbol{e} = [\boldsymbol{\Lambda} \quad \boldsymbol{I}] \begin{bmatrix} \boldsymbol{e}_1 \\ \boldsymbol{e}_2 \end{bmatrix} = \boldsymbol{\Lambda}\boldsymbol{e}_1 + \dot{\boldsymbol{e}}_1, \tag{28}$$

where $\dot{\boldsymbol{e}}$ represents the tracking speed error and:

$$\boldsymbol{\Lambda} = diag[\lambda_1, \ldots, \lambda_n], \quad \lambda_i > 0,$$

that determines the system bandwidth. Next, the time derivative of (28) is taken as follows [18]:

$$\dot{\boldsymbol{s}}(\boldsymbol{e}) = \boldsymbol{\Lambda}\dot{\boldsymbol{e}}_1 + \dot{\boldsymbol{e}}_2 = \boldsymbol{\Lambda}\dot{\boldsymbol{e}}_1 + \ddot{\boldsymbol{q}}^d - \ddot{\boldsymbol{q}}. \tag{29}$$

Now, constant plus proportional rate reaching law as represented by

$$\dot{\boldsymbol{s}} = -\boldsymbol{Q}sgn(s) - \boldsymbol{K}\boldsymbol{s} \tag{30}$$

is adapted. Substituting (30) into (29) and setting $\ddot{\boldsymbol{q}}$ apart yields:

$$\ddot{\boldsymbol{q}} = \boldsymbol{Q}sgn(\boldsymbol{s}) + \boldsymbol{K}\boldsymbol{s} + \boldsymbol{\Lambda}\dot{\boldsymbol{e}}_1 + \ddot{\boldsymbol{q}}^d. \tag{31}$$

Finally, substituting (31) into the non-linear plant of continuous-time dynamic model of robot systems in (8) results in:

$$\boldsymbol{M}(\boldsymbol{q})\left[\boldsymbol{Q}sgn(\boldsymbol{s}) + \boldsymbol{K}\boldsymbol{s} + \boldsymbol{\Lambda}\dot{\boldsymbol{e}}_1 + \ddot{\boldsymbol{q}}^d\right] + \boldsymbol{C}(\boldsymbol{q}, \dot{\boldsymbol{q}})\dot{\boldsymbol{q}} + \boldsymbol{F}(\dot{\boldsymbol{q}}) + \boldsymbol{G}(\boldsymbol{q}) = \boldsymbol{\tau}. \tag{32}$$

This is also known as the *final control law*.

5. Proofs of the boundedness and convergence properties of smooth sliding mode controllers

In this section, the proofs of the boundedness and convergence properties of the smooth sliding mode controllers are introduced. In particular, the convergence analysis of smooth sliding mode controllers will be explained and discussed to the finest detail. Lyapunov's direct method is used to handle the finite-time convergence of the tracking error vector to the boundary layer. Also, once in the boundary layer, the tracking error vector is said to have exponentially converged to a bounded region, as proven analytically.

5.1 Problem statement

Consider the following non-linear system class of n-th order:

$$x^{(n)} = f(\boldsymbol{x}) + b(\boldsymbol{x})u, \tag{33}$$

where u is the control input, $x^{(n)}$, is the n-th order derivative of the interested scalar output variable x with respect to time $t \in [0, \infty)$. Here, also, $\boldsymbol{x} = \left[x, \dot{x}, \ldots, x^{(n-1)}\right]^T$ represents the system state vector, and both $f(x)$ and $b(x)$, such that $f, b : \boldsymbol{R}^n \rightarrow \boldsymbol{R}$, denote nonlinear functions.

The following assumptions will be made in terms of the dynamic system presented in (33).

Assumption 1. *f is an unknown function such that it is bounded by a known function $\boldsymbol{x}$, i.e., $\left|\hat{f}(\boldsymbol{x}) - f(\boldsymbol{x})\right| \leq F(\boldsymbol{x})$, where $\hat{f}$ is an estimate of f.*

Assumption 2. *Input gain $b(\boldsymbol{x})$ is an unknown function such that it is positive and bounded, i.e., $0 < b_{min} \leq b(\boldsymbol{x}) \leq b_{max}$.*

In the proposed state space control problem, the $\boldsymbol{x}$ state vector must be able to follow a desired trajectory $\boldsymbol{x}_d = \left[x_d, \ddot{x}_d, \ldots, x_n^{(n-1)}\right]$, even under the presence of parametric uncertainties and unmodulated dynamics.

The following assumptions should also be made during the development of the control law.

Assumption 3. *The state vector $\boldsymbol{x}$ has availability.*

Assumption 4. *The desired trajectory $\boldsymbol{x}_d$ is differentiated once in time. Moreover, each element of the vector $\boldsymbol{x}_d$ as well as $\boldsymbol{x}_d^{(n)}$, is available and has known bounds.*

Now, let $\tilde{\boldsymbol{x}} = \boldsymbol{x} - \boldsymbol{x}_d$ be defined as the tracking error for the variable x, and $\tilde{\boldsymbol{x}} = \boldsymbol{x} - \boldsymbol{x}_d = \left[\tilde{x}, \dot{\tilde{x}}, \ldots, \tilde{x}^{(n-1)}\right]$ as the tracking error vector.

Let us define a sliding surface S in the state space by the equation $s(\tilde{\boldsymbol{x}}) = 0$ in which s is the function mapping from n-dimensional real space $\boldsymbol{R}^n$ to one-dimensional real space $\boldsymbol{R}$, i.e., $s : \boldsymbol{R}^n \rightarrow \boldsymbol{R}$, and satisfying the following equation:

$$s(\tilde{\boldsymbol{x}}) = \left(\frac{d}{dt} + \lambda\right)^{n-1} \tilde{x},$$

which can be plainly rewritten as

$$s(\tilde{\boldsymbol{x}}) = \boldsymbol{c}^T \tilde{\boldsymbol{x}}, \tag{34}$$

where $\boldsymbol{c} = \left[c_{n-1}\lambda^{n-1} + \ldots + c_1\lambda, c_0\right]$ with c_i representing binomial coefficients as follows:

$$c_i = \binom{n-1}{i} = \frac{(n-1)!}{(n-i-1)!i!}, i = 0, 1, \ldots, n-1 \tag{35}$$

which makes $c_{n-1}\lambda^{n-1} + \ldots + c_1\lambda, c_0$ a Hurwitz polynomial.

It can be easily verified from (35) that $c_0 = 1$, for $\forall n \geq 1$. Therefore, the time derivative of s will be expressed in the following form:

$$\dot{s} = \boldsymbol{c}^T\dot{\tilde{\boldsymbol{x}}} = \underbrace{\begin{bmatrix} c_{n-1}\lambda^{n-1} \\ \vdots \\ c_1\lambda \\ c_0 \end{bmatrix}}_{\boldsymbol{c}^T} \underbrace{\left[\dot{\tilde{x}}, \ddot{\tilde{x}}, \ldots, \tilde{x}^{(n)}\right]}_{\dot{\tilde{\boldsymbol{x}}}} = \underbrace{\begin{bmatrix} 0 \\ c_{n-1}\lambda^{n-1} \\ \vdots \\ c_2\lambda^2 \\ c_1\lambda \end{bmatrix}}_{\triangleq \bar{\boldsymbol{c}}^T} \underbrace{\left[\tilde{x}, \dot{\tilde{x}}, \ldots, \tilde{x}^{(n-1)}\right]}_{\dot{\tilde{\boldsymbol{x}}}} + \tilde{x}^{(n)}$$

i.e.,

$$\dot{s} = \boldsymbol{c}^T\dot{\tilde{\boldsymbol{x}}} = \tilde{x}^{(n)} + \bar{\boldsymbol{c}}^T\tilde{\boldsymbol{x}} \tag{36}$$

where, here, as used for the first time above, there is a definition in the form of $\bar{\boldsymbol{c}} = \left[0, c_{n-1}\lambda^{n-1}, \cdots, c_1\lambda\right]$. At this point, let us evaluate Eqs. (34) and (36) for $n = 3$, i.e.,

$$s(\tilde{\boldsymbol{x}}) = \left(\frac{d}{dt} + \lambda\right)^2 \tilde{x} = \ddot{\tilde{x}} + 2\lambda\dot{\tilde{x}} + \lambda^2\tilde{x},$$

from which $\boldsymbol{c}$ appears to be as $\boldsymbol{c} = \left[c_2\lambda^2, c_1\lambda, c_0\right]$. Then, $s(\tilde{\boldsymbol{x}}) = \boldsymbol{c}^T\tilde{\boldsymbol{x}}$ or to create a polynomial, $\boldsymbol{c}\tilde{\boldsymbol{x}}^T = \left[c_2\lambda^2, c_1\lambda, c_0\right]\begin{bmatrix} \tilde{x} \\ \dot{\tilde{x}} \\ \ddot{\tilde{x}} \end{bmatrix} = c_2\lambda^2\tilde{x} + c_1\lambda\dot{\tilde{x}} + c_0\ddot{\tilde{x}}$ with $c_0 = 1$ as always, and $c_2\lambda^2 + c_1\lambda + c_0$ is a Hurwitz polynomial. That is, it is defined as the polynomial with its coefficients (i.e., c_i) that are positive real numbers, and its zeros are located in the left half-plane –i.e., the real part of every zero is negative– of the complex plane.

Now, Let the problem of controlling the uncertain nonlinear system expressed by (33) be handled for review through the classical sliding mode approach that defines a control rule consisted of an equivalent control $\hat{u} = \hat{b}^{-1}\left(-\hat{f} + x_d^{(n)} - \bar{\boldsymbol{c}}^T\tilde{\boldsymbol{x}}\right)$ and a discontinuous term $-Ksgn(s)$ as follows:

$$u = \hat{b}^{-1}\left(-\hat{f} + x_d^{(n)} - \bar{\boldsymbol{c}}^T\tilde{\boldsymbol{x}}\right) - Ksgn(s). \tag{37}$$

where $\hat{b} = \sqrt{b_{max}b_{min}}$ represents the estimated value of b, and K represents a positive gain. Furthermore, the sign or signum function represented by $sgn\,(s)$ above

$$sgn\,(s) = \begin{cases} -1, & if\ s < 0 \\ 0, & if\ s = 0. \\ 1, & if\ s > 0 \end{cases}$$

Based on Assumptions 1 and 2 given above and taking into account the fact that $\beta^{-1} \le \hat{b}/b \le \beta$, where $\beta = \sqrt{b_{max}/b_{min}}$, the gain K must be determined in such a way as to ensure the following inequality:

$$K \ge \beta\hat{b}^{-1}(\eta + F) + (\beta - 1)\left|\hat{b}^{-1}\left(-\hat{f} + x_d^{(n)} - \bar{\boldsymbol{c}}^T\tilde{\boldsymbol{x}}\right)\right|, \tag{38}$$

where η is a strictly positive constant of the reaching time. Now, in this step, let us reaffirm the validity of the lower and upper bounds of b using the $\hat{b}$ and β

definitions given: first of all, Let the definitions of $\hat{b}$ and β be placed in the expression $\beta^{-1} \le \hat{b}/b \le \beta$ given above. In this case,

$$\frac{1}{\sqrt{b_{max}/b_{min}}} \le \frac{\sqrt{b_{max}b_{min}}}{b} \le \sqrt{b_{max}/b_{min}}.$$

If each side is multiplied by $1/\sqrt{b_{max}b_{min}}$, the following inequality is obtained:

$$\frac{1}{b_{max}} \le \frac{1}{b} \le \frac{1}{b_{min}}.$$

In this inequality, if inversion is applied to all terms, inequalities will be completely displaced, that is to say, it will become $b_{max} \ge b \ge b_{min}$. This is a necessary initial acceptance. Therefore, when we turn b's upper and lower bounds into inequality, we once again confirm the correctness of the definitions for $\hat{b}$ and β. Since the control rule will be designed to be robust against the inequality $\beta^{-1} \le \hat{b}/b \le \beta$, that is, a bounded multiplicative uncertainty, taking advantage of the similarity to the terminology used in linear control, we can call β the gain margin of the design.

In order to ensure $x \equiv x_d$ system tracking, we define a sliding surface $s = 0$ according to $s(\boldsymbol{x}; t) = \left(\frac{d}{dt} + \lambda\right)^{n-1}\tilde{x}$, that is,

$$s = \left(\frac{d}{dt} + \lambda\right)\tilde{x} = \dot{\tilde{x}} + \lambda\tilde{x}.$$

When we derive the expression s, we obtain the following:

$$\dot{s} = \ddot{\tilde{x}} + \lambda\dot{\tilde{x}} = \ddot{x} - \ddot{x}_d + \lambda\dot{\tilde{x}} = f + u - \ddot{x}_d + \lambda\dot{\tilde{x}}.$$

For $\dot{s} = f + u - \ddot{x}_d + \lambda\dot{\tilde{x}} = 0$ to be realized, other terms outside of u must be determined equal to the opposite sign of $\hat{u}$, which is the best approximation of a continuous control rule u that can implement $\dot{s} = 0$, that is,

$$\hat{u} = -\hat{f} + \ddot{x}_d - \lambda\dot{\tilde{x}}.$$

In fact, to see this result, the first thing to do is to draw u from the equation $\dot{s} = f + u - \ddot{x}_d + \lambda\dot{\tilde{x}} = 0$. Hence, $u = -f + \ddot{x}_d - \lambda\dot{\tilde{x}}$ is obtained. Then, from here, in order to obtain the approximate value of u, searching for the approximation of the function on the right side of the equation, and representing this approximated function by $\hat{f}$ symbolically are sufficient to lead us to the correct result, as seen above.

The control rule $u = \hat{b}^{-1}[\hat{u} - ksgn(s)]$ with predefined s and $\hat{u}$, and k defined by the inequality $k \ge \beta(F + \eta) + (\beta - 1)|\hat{u}|$—as will be explained little below—meets the sliding condition. Indeed, when we substitute this control rule in the expression $\dot{s} = f + bu - \ddot{x}_d + \lambda\dot{\tilde{x}}$ by choosing the use of $\ddot{x} = f + bu$, which is more specific to this type of structure, instead of $\ddot{x} = f + u$ used only just two above, we obtain the following,

$$\dot{s} = f + b\hat{b}^{-1}[\hat{u} - ksgn(s)] - \ddot{x}_d + \lambda\dot{\tilde{x}}.$$

Once the previously determined $\hat{u}$ is replaced above, the following equation is reached:

$$\dot{s} = f + b\hat{b}^{-1}\left[-\hat{f} + \ddot{x}_d - \lambda\dot{\tilde{x}} - ksgn(s)\right] - \ddot{x}_d + \lambda\dot{\tilde{x}}.$$

The organized form of this statement will be as follows:

$$\dot{s} = \left(f - b\hat{b}^{-1}\hat{f}\right) + \left(1 - b\hat{b}^{-1}\right)\left(-\ddot{x}_d + \lambda\dot{\tilde{x}}\right) - b\hat{b}^{-1}ksgn(s).$$

Such that k should meet the following condition,

$$k \geq \left|\hat{b}b^{-1}f - \hat{f} + \left(\hat{b}b^{-1} - 1\right)\left(-\ddot{x}_d + \lambda\dot{\tilde{x}}\right)\right| + \eta\hat{b}b^{-1} \tag{39}$$

We can really achieve this condition by following the steps below:

$$\dot{s} = 0 = \left(f - b\hat{b}^{-1}\hat{f}\right) + \left(1 - b\hat{b}^{-1}\right)\left(-\ddot{x}_d + \lambda\dot{\tilde{x}}\right) - b\hat{b}^{-1}ksgn(s) \Longrightarrow$$

$$b\hat{b}^{-1}ksgn(s) = \left(f - b\hat{b}^{-1}\hat{f}\right) + \left(1 - b\hat{b}^{-1}\right)\left(-\ddot{x}_d + \lambda\dot{\tilde{x}}\right) \Longrightarrow$$

$$ksgn(s) = \hat{b}b^{-1}f - \hat{f} + \left(\hat{b}b^{-1} - 1\right)\left(-\ddot{x}_d + \lambda\dot{\tilde{x}}\right) \Longrightarrow$$

$$ksgn(s) = \hat{b}b^{-1}\left[\hat{f} + \left(f - \hat{f}\right)\right] - \hat{f} + \left(\hat{b}b^{-1} - 1\right)\left(-\ddot{x}_d + \lambda\dot{\tilde{x}}\right).$$

Here, it was previously described that $\left|f - \hat{f}\right| \leq F$. But, when determining k, it will be necessary to take into account the *reaching time* η. Therefore, we will allow $F + \eta$ to be written instead of F. Removing the term $sgn(s)$, k will be determined as follows as a result of our compensation through expressing, with an absolute value, the effect of its reciprocations being of which the negative s values relative to the positive s values and of which only the sign changed:

$$k \geq \hat{b}b^{-1}F + \eta\hat{b}b^{-1} + \left|\hat{b}b^{-1} - 1\right|\left|\hat{f} - \ddot{x}_d + \lambda\dot{\tilde{x}}\right|.$$

Note here that $F \geq 0$ and $\eta > 0$ (absolute positive). For this reason, there is no need to take absolute values of these terms. Here again, using the definition $\hat{b}b^{-1} \triangleq \beta$, for k, we get the expression,

$$k \geq \beta(F + \eta) + |\beta - 1||\hat{u}|. \tag{40}$$

Remark 1. To avoid any confusion, if we wanted to verify (40) by proceeding from (39), since η has already been taken into account in (39), we would not need to take $F + \eta$ instead of F. We would proceed directly with $\left|f - \hat{f}\right| \leq F$.

Remark 2. Considering the fact that the F value can be faced with moments where the estimation problem will be relatively large by nature and similarly with the moments when η reaching time will be relatively larger, it is possible to state precisely that it is the right choice or necessity to take the direction of inequality k greater than or equal to.

Thus, it can be easily verified that the control rule $u = \hat{b}^{-1}\left(-\hat{f} + x_d^{(n)} - \bar{\boldsymbol{c}}^T\tilde{\boldsymbol{x}}\right) - Ksgn(s)$ is sufficient to impose the shift condition,

$$\frac{1}{2}\frac{d}{dt}s^2 \leq -\eta|s|,$$

which indeed guarantees the convergence of the tracking error vector to the sliding surface S and consequently its exponential stability in a finite-time. In response to the uncertainty of f on dynamics, we add a discontinuous term to $\hat{u}$ across the surface $s = 0$ to meet the slip condition given above, that is:

$$u = \hat{u} - ksgn(s).$$

Here we can now guarantee that the sliding condition will be verified by choosing $k = k(x, \dot{x})$ sufficiently large. Indeed,

$$\frac{1}{2}\frac{d}{dt}s^2 = \dot{s}s = \left[f + \hat{u} - ksgn(s) - \ddot{x}_d + \lambda\dot{\tilde{x}}\right]s = \left[f - \hat{f} - ksgn(s)\right]s.$$

This last operation is important; because we have reached this point by using the equations $u = -f + \ddot{x}_d - \lambda\dot{\tilde{x}}$, $\hat{u} = -\hat{f} + \ddot{x}_d - \lambda\dot{\tilde{x}}$, and $u = \hat{u} - ksgn(s)$ as follows:

$$\begin{aligned}\dot{s} &= \left[f + u - \ddot{x}_d + \lambda\dot{\tilde{x}}\right] = f + \hat{u} - ksgn(s) - \ddot{x}_d + \lambda\dot{\tilde{x}} \\ &= f + \left(-\hat{f} + \ddot{x}_d - \lambda\dot{\tilde{x}}\right) - ksgn(s) - \ddot{x}_d + \lambda\dot{\tilde{x}} = f - \hat{f} - ksgn(s).\end{aligned}$$

If we continue where we were,

$$\frac{1}{2}\frac{d}{dt}s^2 = \left[f - \hat{f} - ksgn(s)\right]s = \left(f - \hat{f}\right)s - ksgn(s)s.$$

Therefore, since $sgn\,(s)s = |s|$, the following expression is reached,

$$\frac{1}{2}\frac{d}{dt}s^2 = \dot{s}s = \left[f - \hat{f} - ksgn(s)\right]s = \left(f - \hat{f}\right)s - k|s|.$$

So that, when $k = F + \eta$ is selected, the above statement follows,

$$\frac{1}{2}\frac{d}{dt}s^2 = \dot{s}s = \left(f - \hat{f}\right)s - F|s| - \eta|s|.$$

However, although the definition of $\left|\hat{f} - f\right| \leq F$ is given at the beginning of the section, recalling that we prefer the form $\left|f - \hat{f}\right| \leq F$ to be used in the case study below, Let us give the statement its final form:

$$\frac{1}{2}\frac{d}{dt}s^2 = \dot{s}s = \left(f - \hat{f}\right)s - \left|f - \hat{f}\right||s| - \eta|s|. \tag{41}$$

In fact, note that here the expression $\left|f - \hat{f}\right|$, which we substitute for F represents the smallest value that F can take. We generally know that F is greater than this value.

We will now carry out the following case studies for the Eq. (41):

Case 1. *If* $\left(f - \hat{f}\right)$ *and s are both negative or positive, as such,* $\left(f - \hat{f}\right)s - \left|f - \hat{f}\right||s| = 0$. *However, it is known to be* $F \geq \left|f - \hat{f}\right|$, *hence,* $\left(f - \hat{f}\right)s - F|s| \leq 0$, *i.e., it will always be negative.*

Case 2. *However, if* $\left(f-\hat{f}\right)$ *and s opposite signs;* $\left(f-\hat{f}\right)s$ *will always be negative.* $-F|s|$ *will also be negative. Hence,* $\left(f-\hat{f}\right)s-F|s|$ *will always be more negative as compared to Case 1.*

As a result,

$$\frac{1}{2}\frac{d}{dt}s^2 \leq -\eta|s|,$$

is always true.

However, the presence of a discontinuous term (i.e., $-Ksgn(s)$) in the control rule leads to the well-known *chattering* effect. To prevent these unwanted high-frequency oscillations of the controlled variable, Slotine had proposed the idea of adopting a thin boundary layer $S_{\varnothing}$ around the switching surface [1]:

$$S_{\varnothing} = \{\tilde{\boldsymbol{x}} \in \boldsymbol{R}^n \,||s(\tilde{\boldsymbol{x}})| \leq \varnothing\}. \tag{42}$$

Here $\varnothing$ is an absolute positive constant, which represents the boundary layer thickness.

The boundary layer is accomplished by replacing the sign function with a continuous interpolation in $S_{\varnothing}$. It should be emphasized that this smooth approximation referring to the flatness or smoothness of the interpolating curve and its derivatives, which will be called $\varphi(s,\varnothing)$, here, will definitely act as a sign function outside the boundary layer.

Various options are available to smooth out the ideal switch. But the closest choices are the saturation function expressed by

$$sat\left(\frac{s}{\varnothing}\right) = \begin{cases} sgn\,(s), if \left|\frac{s}{\varnothing}\right| \geq 1 \\ \frac{s}{\varnothing}, if \left|\frac{s}{\varnothing}\right| < 1, \end{cases} \tag{43}$$

and the hyperbolic tangent function expressed by $tanh\left(\frac{s}{\varnothing}\right)$. Thus, the smooth sliding mode control rule can be expressed as follows:

$$u = \hat{b}^{-1}\left(-\hat{f} + x_d^{(n)} - \bar{\boldsymbol{c}}^T\tilde{\boldsymbol{x}}\right) - K\varphi(s,\varnothing). \tag{44}$$

5.2 Convergence analysis

The attractiveness and invariance properties of the boundary layer are introduced in the following theorem:

Theorem 1. Consider four previously made assumptions with the uncertain nonlinear system given in (33). Therefore, the smooth sliding mode controller defined by (38) and (44) provides the finite-time convergence of the tracking error vector to the boundary layer $S_{\varnothing}$ defined by (42).

Proof. Let a positive-definite Lyapunov function candidate V be defined as,

$$V(t) = \frac{1}{2}{s_{\varnothing}}^2. \tag{45}$$

Here, as a measure of the distance of the current error to the boundary layer, $s_{\varnothing}$ can be computed as follows:

$$s_{\varnothing} = s - \varnothing sat\left(\frac{s}{\varnothing}\right). \tag{46}$$

Noting that $s_{\varnothing} = 0$ in the boundary layer, it is shown that $\dot{V}(t) = 0$ inside $S_{\varnothing}$. It is also possible to easily verify that $\dot{s}_{\varnothing} = \dot{s}$ outside the boundary layer through (43) and (46), and in this case, $\dot{V}$ can be written as follows:

$$\begin{aligned}\dot{V}(t) &= s_{\varnothing}\dot{s}_{\varnothing} = s_{\varnothing}\dot{s} = s_{\varnothing}\left(\boldsymbol{c}^T\dot{\tilde{\boldsymbol{x}}}\right) = s_{\varnothing}\left(\tilde{x}^{(n)} + \bar{\boldsymbol{c}}^T\tilde{\boldsymbol{x}}\right) = \left(x^{(n)} - x_d^{(n)} + \bar{\boldsymbol{c}}^T\tilde{\boldsymbol{x}}\right)s_{\varnothing} \\ &= \left(f + bu - x_d^{(n)} + \bar{\boldsymbol{c}}^T\tilde{\boldsymbol{x}}\right)s_{\varnothing}.\end{aligned}$$

Next, considering that the control rule given by (44) is written as

$$u = \hat{b}^{-1}\left(-\hat{f} + x_d^{(n)} - \bar{\boldsymbol{c}}^T\tilde{\boldsymbol{x}}\right) - Ksgn(s_{\varnothing}),$$

outside the boundary layer and noting that $f = \hat{f} - \left(\hat{f} - f\right)$, we get the following result:

$$\dot{V}(t) = -\left[\left(\hat{f} - f\right) - b\hat{b}^{-1}\left(-\hat{f} + x_d^{(n)} - \bar{\boldsymbol{c}}^T\tilde{\boldsymbol{x}}\right) - \hat{f} + x_d^{(n)} - \bar{\boldsymbol{c}}^T\tilde{\boldsymbol{x}} + bKsgn(s_{\varnothing})\right]s_{\varnothing}.$$

Thus, by taking the Assumptions 1 and 2 into consideration, and defining K according to (38), $\dot{V}$ can be written as follows,

$$\dot{V}(t) \leq -\eta|s_{\varnothing}|.$$

Because the Lyapunov function candidate, which we initially defined with (45) as positive definite, essentially inspired by the inequality in the form of $\frac{1}{2}\frac{d}{dt}s^2 \leq -\eta|s|$ which we have always correctly demonstrated above, may well be represented by a similar structure to the form, $\frac{1}{2}\frac{d}{dt}{s_{\varnothing}}^2 \leq -\eta|s_{\varnothing}|$. It will be seen from here that $\dot{V}(t) = s_{\varnothing}\dot{s}_{\varnothing} \leq -\eta|s_{\varnothing}|$, as well. Hence, the inequality $\dot{V}(t) \leq -\eta|s_{\varnothing}|$ will imply that $V(t) \leq V(0)$ and therefore $s_{\varnothing}$ is bounded. Moreover, from the definitions of s and $s_{\varnothing}$ expressed in (35) and (46), respectively, it can be verified that $\tilde{\boldsymbol{x}}$ is bounded. Therefore, Assumption 4 and (36) imply that $\dot{s}$ is also bounded.

Finite-time convergence of the tracking error vector to the boundary layer can be shown remembering the expression,

$$\dot{V}(t) = \frac{1}{2}\frac{d}{dt}{s_{\varnothing}}^2 = s_{\varnothing}\dot{s}_{\varnothing} \leq -\eta|s_{\varnothing}|.$$

Then, dividing both sides into $|s_{\varnothing}|$ above and integrating them between 0 and t will refer to the following result:

$$\int_0^t \frac{s_{\varnothing}}{|s_{\varnothing}|}\dot{s}_{\varnothing}d\tau \leq -\int_0^t \eta d\tau.$$

Remark 3. Here, considering the ratio $s_{\varnothing}/|s_{\varnothing}|$ as the ratio of two numbers of the same size and therefore assuming it disappeared, that is, since it has no effect in

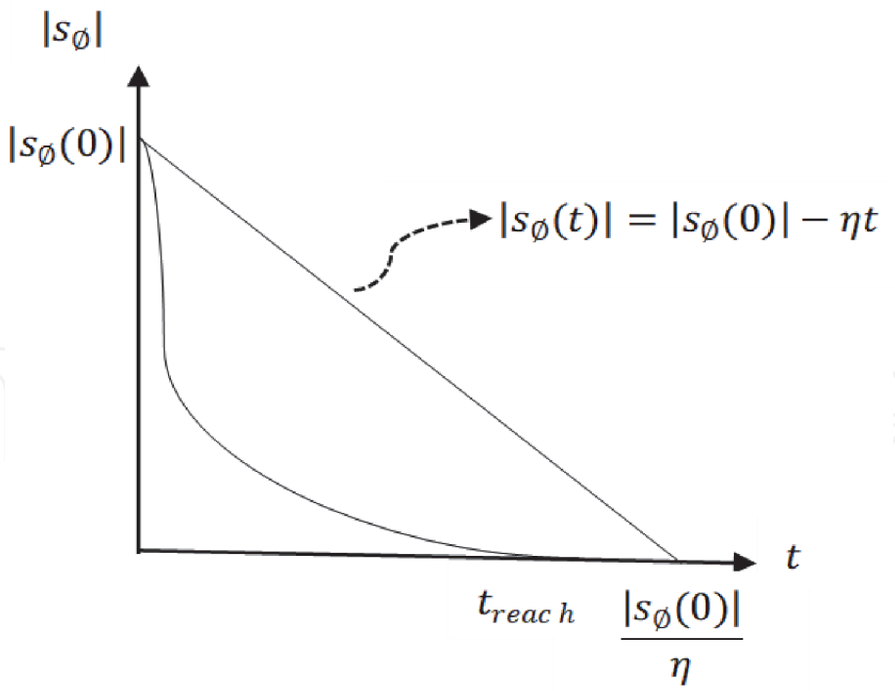

Figure 7.
Time evolution of the distance of the current tracking error to the boundary layer $|s_\emptyset|$.

size, substantially it is a correct approach to consider the integral as an equivalent to $\int_0^t \dot{s}_\emptyset d\tau$. This produces the result $|s_\emptyset(t)||_0^t$. Consequently, knowing the fact that in the situation before taking this approach, the product $s_\emptyset \dot{s}_\emptyset$ which appears in the numerator of the integral to the left of inequality is essentially equal to the derivative of the positive-definite V Lyapunov candidate function and is therefore positive again, it is essential to show the terms on the left side of the inequality with absolute value. That is to say, it is important to see that $\frac{s_\emptyset \dot{s}_\emptyset}{|s_\emptyset|} > 0$. Then, the next step to ensure this will turn into the form $|s_\emptyset(t)| - |s_\emptyset(0)| \leq -\eta t$. In this way, considering t_{reach} as the time required to reach $s_\emptyset$ and noting that $|s_\emptyset(t_{reach})| = 0$, we have the expression,

$$t_{reach} \leq \frac{|s_\emptyset(0)|}{\eta}$$

guaranteeing the convergence of the tracking error vector to the boundary layer in a time interval less than $|s_\emptyset(0)|/\eta$.

Remark 4. If both sides of $|s_\emptyset(t)| - |s_\emptyset(0)| \leq -\eta t$ are multiplied by -1, $|s_\emptyset(0)| - |s_\emptyset(t)| \geq \eta t$ is obtained, that is, briefly, the inequality is displaced. If t is left alone in the next step, $t \leq \frac{|s_\emptyset(0)| - |s_\emptyset(t)|}{\eta}$ is obtained. Hence, it is guaranteed to be $t_{reach} \leq |s_\emptyset(0)|/\eta$. That is, the right-hand side will act as the largest value achievable for t_{reach}. In other words, it will appear as a guaranteed upper value. Then, the value of $\frac{|s_\emptyset(0)| - |s_\emptyset(t)|}{\eta}$ is expected to be less than this guaranteed value of $|s_\emptyset(0)|/\eta$.

Therefore, to keep the reaching time, t_{reach}, as short as possible, the value of the positive constant η can be chosen appropriately. We clearly see from **Figure 7** that the time evolution of $|s_\emptyset|$ is bounded by the linear equation $|s_\emptyset(t)| = |s_\emptyset(0)| - \eta t$.

Lastly, the proof of the boundedness of the tracking error vector is based on Theorem 2.

Theorem 2. Let the boundary layer $S_\emptyset$ be defined according to (42). Then, once inside $S_\emptyset$, the tracking error vector will exponentially converge to an n-dimensional box defined according to $\left|\tilde{x}^{(i)}\right| \leq \zeta_i \lambda^{i-n+1} \phi, i = 0, 1, \cdots, n-1,$ with ζ_i satisfying

$$\zeta_i = \begin{cases} 1, for\, i = 0 \\ 1 + \sum_{j=0}^{i-1} \binom{i}{j} \zeta_j, for\, i = 1, 2, \cdots, n-1. \end{cases} \tag{47}$$

Proof. Considering the fact that $|s(\tilde{\boldsymbol{x}})| \leq \varnothing$ can be rewritten as $-\varnothing \leq s(\tilde{\boldsymbol{x}}) \leq \varnothing$ with the definition of s given in (34), the expression below

$$\begin{aligned} s(\tilde{\boldsymbol{x}}) = \boldsymbol{c}^T \tilde{\boldsymbol{x}} &= \left[c_{n-1}\lambda^{n-1} + \ldots + c_1\lambda, c_0\right] \begin{bmatrix} \tilde{x} \\ \dot{\tilde{x}} \\ \vdots \\ \tilde{x}^{(n-1)} \end{bmatrix} \\ &= c_0\tilde{x}^{(n-1)} + c_1\lambda\tilde{x}^{(n-2)} + \cdots + c_{n-1}\lambda^{n-1}\tilde{x}. \end{aligned}$$

Thus,

$$-\varnothing \leq s(\tilde{\boldsymbol{x}}) \leq \varnothing = -\varnothing \leq c_0\tilde{x}^{(n-1)} + c_1\lambda\tilde{x}^{(n-2)} + \cdots + c_{n-1}\lambda^{n-1}\tilde{x} \leq \varnothing, \tag{48}$$

or the following,

$$-\varnothing \leq \left(\frac{d}{dt} + \lambda\right)^{n-1} \tilde{x} \leq \varnothing \tag{49}$$

can be written. If (49) is multiplied by $e^{\lambda t}$, the following statement is reached:

$$-\varnothing e^{\lambda t} \leq \left(\frac{d}{dt} + \lambda\right)^{n-1} \tilde{x}e^{\lambda t} \leq \varnothing e^{\lambda t}.$$

In fact, this expression is equal to

$$-\varnothing e^{\lambda t} \leq \frac{d^{n-1}}{dt^{n-1}}\left(\tilde{x}e^{\lambda t}\right) \leq \varnothing e^{\lambda t}. \tag{50}$$

That is to say,

$$\left(\frac{d}{dt} + \lambda\right)^{n-1} \tilde{x}e^{\lambda t} = \frac{d^{n-1}}{dt^{n-1}}\left(\tilde{x}e^{\lambda t}\right). \tag{51}$$

We can confirm this form of (51) for small n values. Namely, if binomial expansion is applied for $\left(\frac{d}{dt} + \lambda\right)^{n-1}$,

$$\left(\frac{d}{dt} + \lambda\right)^{n-1} = \sum_{k=0}^{n-1} \binom{n-1}{k} \frac{d^k}{dt^k} \lambda^{n-1-k}$$

is written. Hence,

$$s(\tilde{\boldsymbol{x}}) = \left(\frac{d}{dt} + \lambda\right)^{n-1} \tilde{x} = \sum_{k=0}^{n-1} \binom{n-1}{k} \frac{d^k\tilde{x}}{dt^k} \lambda^{n-1-k}. \tag{52}$$

At this point, we can make a confirmation by taking $n = 3$:

For $n = 1$, it becomes $s(\tilde{\boldsymbol{x}}) = \begin{pmatrix} 0 \\ 0 \end{pmatrix} \frac{d^0\tilde{x}}{dt^0}\lambda^0 = \tilde{x}$. The binomial coefficient of this single term is 1, and this number is at the top of the Pascal triangle. For $n = 2$, it becomes $s(\tilde{\boldsymbol{x}}) = \begin{pmatrix} 1 \\ 0 \end{pmatrix} \frac{d^0\tilde{x}}{dt^0}\lambda^{1-0} + \begin{pmatrix} 1 \\ 1 \end{pmatrix} \frac{d\tilde{x}}{dt}\lambda^{1-1} = \lambda\tilde{x} + \frac{d\tilde{x}}{dt}$. Here, the coefficients of both terms are 1. It gives the numbers of one-down row from the top of the Pascal triangle. For $n = 3$, it becomes

$$s(\tilde{\boldsymbol{x}}) = \begin{pmatrix} 2 \\ 0 \end{pmatrix} \frac{d^0\tilde{x}}{dt^0}\lambda^{2-0} + \begin{pmatrix} 2 \\ 1 \end{pmatrix} \frac{d\tilde{x}}{dt}\lambda^{2-1} + \begin{pmatrix} 2 \\ 2 \end{pmatrix} \frac{d^2\tilde{x}}{dt^2}\lambda^{2-2} = \lambda^2\tilde{x} + 2\lambda\frac{d\tilde{x}}{dt} + \frac{d^2\tilde{x}}{dt^2}. \quad (53)$$

Here, the coefficients of the three terms from left to right are 1, 2, 1. This gives the elements of the two-down row from the top of the Pascal triangle. If the expression $-\varnothing \le s(\tilde{\boldsymbol{x}}) \le \varnothing$ is multiplied by $e^{\lambda t}$,

$$-\varnothing e^{\lambda t} \le s(\tilde{\boldsymbol{x}})e^{\lambda t} \le \varnothing e^{\lambda t}$$

is obtained. If the result for $n = 3$ in Eq. (52), or its equivalent (53) is substituted above,

$$-\varnothing e^{\lambda t} \le \left(\lambda^2 e^{\lambda t}\tilde{x} + 2\lambda e^{\lambda t}\frac{d\tilde{x}}{dt} + e^{\lambda t}\frac{d^2\tilde{x}}{dt^2}\right) \le \varnothing e^{\lambda t},$$

or the following expression is obtained:

$$-\varnothing e^{\lambda t} \le \frac{d^2}{dt^2}\left(e^{\lambda t}\tilde{x}\right) \le \varnothing e^{\lambda t}.$$

This verifies the multiplication of $s(\tilde{\boldsymbol{x}})$ with $e^{\lambda t}$ for $n = 3$. In other words, the equation $\left(\frac{d}{dt} + \lambda\right)^2 \tilde{x}e^{\lambda t} = \frac{d^2}{dt^2}\left(\tilde{x}e^{\lambda t}\right)$ is satisfied. Once this statement is generalized for n, the validity of Eq. (51) is proven.

If the inequality (50) is integrated between 0 and t,

$$-\int_0^t \varnothing e^{\lambda\tau} d\tau \le \int_0^t \frac{d^{n-1}}{dt^{n-1}}\left(\tilde{x}e^{\lambda t}\right) d\tau \le \int_0^t \varnothing e^{\lambda t} d\tau,$$

and one step later,

$$-\frac{\varnothing}{\lambda}e^{\lambda\tau}\Big|_0^t \le \frac{d^{n-2}}{dt^{n-2}}\left(\tilde{x}e^{\lambda\tau}\right)\Big|_0^t \le \frac{\varnothing}{\lambda}e^{\lambda\tau}\Big|_0^t,$$

and finally the following expression is reached:

$$\frac{-\varnothing}{\lambda}e^{\lambda t} + \frac{\varnothing}{\lambda} \le \frac{d^{n-2}}{dt^{n-2}}\left(\tilde{x}e^{\lambda t}\right) - \frac{d^{n-2}}{dt^{n-2}}\left(\tilde{x}e^{\lambda t}\right)\Big|_{t=0} \le \frac{\varnothing}{\lambda}e^{\lambda t} - \frac{\varnothing}{\lambda}.$$

When the term $\frac{d^{n-2}}{dt^{n-2}}\left(\tilde{x}e^{\lambda t}\right)\Big|_{t=0}$ is added to each side of this expression, it takes the form below:

$$\frac{-\varnothing}{\lambda}e^{\lambda t}+\frac{\varnothing}{\lambda}+\frac{d^{n-2}}{dt^{n-2}}\left(\tilde{x}e^{\lambda t}\right)\Big|_{t=0}\leq\frac{d^{n-2}}{dt^{n-2}}\left(\tilde{x}e^{\lambda t}\right)\leq\frac{\varnothing}{\lambda}e^{\lambda t}-\frac{\varnothing}{\lambda}+\frac{d^{n-2}}{dt^{n-2}}\left(\tilde{x}e^{\lambda t}\right)\Big|_{t=0}. \quad (54)$$

Since we can always write,

$$\frac{d^{n-2}}{dt^{n-2}}\left(\tilde{x}e^{\lambda t}\right)\Big|_{t=0}\geq-\left|\frac{d^{n-2}}{dt^{n-2}}\left(\tilde{x}e^{\lambda t}\right)\Big|_{t=0}\right. \text{ and } \frac{d^{n-2}}{dt^{n-2}}\left(\tilde{x}e^{\lambda t}\right)\Big|_{t=0}\leq\left|\frac{d^{n-2}}{dt^{n-2}}\left(\tilde{x}e^{\lambda t}\right)\Big|_{t=0}\right.$$

as a result of replacing the derivative terms in the inequality (54) with their equivalents expressed with an absolute value one above, the inequality conditions will be preserved exactly as the term with the absolute value will be smaller than the term that satisfies the "less than or equal to" condition on the left and greater than the term that provides "greater than or equal to" condition on the right in the equality (54). Furthermore, aside from the absence of a violation, the conditions of inequality have been further reinforced. Therefore, it is possible to write the following under these conditions,

$$\frac{-\varnothing}{\lambda}e^{\lambda t}+\frac{\varnothing}{\lambda}-\left|\frac{d^{n-2}}{dt^{n-2}}\left(\tilde{x}e^{\lambda t}\right)\Big|_{t=0}\right.\leq\frac{d^{n-2}}{dt^{n-2}}\left(\tilde{x}e^{\lambda t}\right)\leq\frac{\varnothing}{\lambda}e^{\lambda t}-\frac{\varnothing}{\lambda}+\left|\frac{d^{n-2}}{dt^{n-2}}\left(\tilde{x}e^{\lambda t}\right)\Big|_{t=0}\right..$$

Also, since both $\varnothing$ and λ are initially defined as positive definite constants, we take $-\varnothing/\lambda$ instead of the leftmost $\varnothing/\lambda$ and $\varnothing/\lambda$ instead of the rightmost $-\varnothing/\lambda$, which can be more safely adapted to existing inequality conditions without loss of generality will be preferred at this stage. Hence, the inequality (54) will turn into a rewritten appropriate form given below:

$$\frac{-\varnothing}{\lambda}e^{\lambda t}-\left(\left|\frac{d^{n-2}}{dt^{n-2}}\left(\tilde{x}e^{\lambda t}\right)\Big|_{t=0}\right.+\frac{\varnothing}{\lambda}\right)\leq\frac{d^{n-2}}{dt^{n-2}}\left(\tilde{x}e^{\lambda t}\right)\leq\frac{\varnothing}{\lambda}e^{\lambda t}+\left(\left|\frac{d^{n-2}}{dt^{n-2}}\left(\tilde{x}e^{\lambda t}\right)\Big|_{t=0}\right.+\frac{\varnothing}{\lambda}\right).$$

The same reasoning can be applied repeatedly until the $(n-1)th$ integral is reached on the inequality (50). Once (50) is integrated, recall that (54) is obtained. If we apply a second integral on (54) or, alternatively, a first integral to the form of (54) given immediately above, the following expression is obtained:

$$\underbrace{-\int_0^t\frac{\varnothing}{\lambda}e^{\lambda t}dt}_{Part(a)}-\underbrace{\int_0^t\left(\left|\frac{d^{n-2}}{dt^{n-2}}\left(\tilde{x}e^{\lambda t}\right)\Big|_{t=0}\right.+\frac{\varnothing}{\lambda}\right)dt}_{Part(b)}\leq\underbrace{\int_0^t\frac{d^{n-2}}{dt^{n-2}}\left(\tilde{x}e^{\lambda t}\right)dt}_{Part(c)}\leq\underbrace{\int_0^t\frac{\varnothing}{\lambda}e^{\lambda t}dt}_{Part(a)}$$
$$+\underbrace{\int_0^t\left(\left|\frac{d^{n-2}}{dt^{n-2}}\left(\tilde{x}e^{\lambda t}\right)\Big|_{t=0}\right.+\frac{\varnothing}{\lambda}\right)dt}_{Part(b)}.$$

In determining the generalized cases below, we would like to state in advance that we do not focus on other terms that will appear in the shape of increasing powers of t in the form of $\frac{t^n}{n!}$ especially in Parts (a) and (c), and we do not show them in the generalized statements. For that matter, as shown a little below, if Eq. (55) is divided by $e^{\lambda t}$ and the limit is taken as t goes to infinity (i.e., $t\rightarrow\infty$), those terms will eventually disappear completely, since the denominator will go to infinity faster than the numerator. After this essential explanation,

For *Part (a)*:

$$\int_0^t \frac{\varnothing}{\lambda} e^{\lambda t} dt = \frac{\varnothing}{\lambda^2} e^{\lambda t}\Big|_0^t = \frac{\varnothing}{\lambda^2} e^{\lambda t} - \frac{\varnothing}{\lambda^2}, n = 2(\textit{for the 2nd integral})$$

$$\frac{\varnothing}{\lambda^3} e^{\lambda t} - \frac{\varnothing}{\lambda^3}, n = 3(\textit{for the 3rd integral})$$

$$\vdots$$

$$\vdots$$

$$\frac{\varnothing}{\lambda^{n-2}} e^{\lambda t} - \frac{\varnothing}{\lambda^{n-2}}, n = n-2(\textit{for the}(n-2)\textit{th integral})$$

$$\frac{\varnothing}{\lambda^{n-1}} e^{\lambda t} - \frac{\varnothing}{\lambda^{n-1}}, n = n-1(\textit{for the}\ (n-1)\textit{th integral}: \textit{Generalized form})$$

For *Part (b)*:

$$\int_0^t \left(\overbrace{\left| \frac{d^{n-2}}{dt^{n-2}} \left(\tilde{x} e^{\lambda t} \right) \right|_{t=0}}^{constant} + \overbrace{\frac{\varnothing}{\lambda}}^{constant} \right) dt = \left(\left| \frac{d^{n-2}}{dt^{n-2}} \left(\tilde{x} e^{\lambda t} \right) \right|_{t=0} + \frac{\varnothing}{\lambda} \right) * t, n$$

$$= 2(\textit{for the 2nd integral})$$

$$\frac{\left(\left| \frac{d}{dt^{n-2}} \left(\tilde{x} e^{\lambda t} \right) \right|_{t=0} + \frac{\varnothing}{\lambda} \right) * t^2}{2}, n = 3(\textit{for the 3rd integral})$$

$$\frac{\left(\left| \frac{d}{dt^{n-2}} \left(\tilde{x} e^{\lambda t} \right) \right|_{t=0} + \frac{\varnothing}{\lambda} \right) * t^3}{6}, n = 4(\textit{for the 4th integral})$$

$$\vdots$$

$$\vdots$$

$$\frac{\left(\left| \frac{d}{dt^{n-2}} \left(\tilde{x} e^{\lambda t} \right) \right|_{t=0} + \frac{\varnothing}{\lambda} \right) * t^{n-3}}{(n-3)!}, n = n-2(\textit{for the}\ (n-2)\textit{th integral})$$

$$\frac{\left(\left| \frac{d}{dt^{n-2}} \left(\tilde{x} e^{\lambda t} \right) \right|_{t=0} + \frac{\varnothing}{\lambda} \right) * t^{n-2}}{(n-2)!}, n = n-1(\textit{for the}\ (n-1)\textit{th integral: Generalized form})$$

For *Part (c)*:

Starting with (50), when the term in the middle of inequality, $\frac{d^{n-1}}{dt^{n-1}} \left(\tilde{x} e^{\lambda t} \right)$, is integrated $(n-1)$ times in a row, it is obvious that only the result, $\tilde{x} e^{\lambda t}$, will be found. Therefore,

$$\int_0^t \frac{d^{n-1}}{dt^{n-1}} \left(\tilde{x} e^{\lambda t} \right) dt = \frac{d^{n-2}}{dt^{n-2}} \left(\tilde{x} e^{\lambda t} \right)\Big|_0^t = \frac{d^{n-2}}{dt^{n-2}} \left(\tilde{x} e^{\lambda t} \right) - \frac{d^{n-2}}{dt^{n-2}} \left(\tilde{x} e^{\lambda t} \right)\Big|_{t=0}, n = 1(1st\ integral)$$

$$\int_0^t \frac{d^{n-2}}{dt^{n-2}} \left(\tilde{x} e^{\lambda t} \right) dt = \frac{d^{n-3}}{dt^{n-3}} \left(\tilde{x} e^{\lambda t} \right)\Big|_0^t = \frac{d^{n-3}}{dt^{n-3}} \left(\tilde{x} e^{\lambda t} \right) - \frac{d^{n-3}}{dt^{n-3}} \left(\tilde{x} e^{\lambda t} \right)\Big|_{t=0}, n = 2(2nd\ integral)$$

$$\vdots$$

$$\vdots$$

$$\int_0^t \frac{d^2}{dt^2}\left(\tilde{x}e^{\lambda t}\right)dt = \frac{d}{dt}\left(\tilde{x}e^{\lambda t}\right)\Big|_0^t = \frac{d}{dt}\left(\tilde{x}e^{\lambda t}\right) - \frac{d}{dt}\left(\tilde{x}e^{\lambda t}\right)\Big|_{t=0}, n = n-2((n-2)th\ integral)$$

$$\int_0^t \frac{d}{dt}\left(\tilde{x}e^{\lambda t}\right)dt = \tilde{x}e^{\lambda t}\Big|_0^t = \tilde{x}e^{\lambda t} - \tilde{x}(0), n-1((n-1)th\ integral)$$

is written. However, due to the reason we have explained above, we would like to remind that we do not take into account other terms that will appear in the shape of increasing powers of t in the form of $\frac{t^n}{n!}$ once again. Therefore, when the determinated generalized terms are put in place,

$$\frac{-\varnothing}{\lambda^{n-1}}e^{\lambda t} + \frac{\varnothing}{\lambda^{n-1}} - \frac{\left(\left|\frac{d}{dt^{n-2}}\left(\tilde{x}e^{\lambda t}\right)\right|_{t=0} + \frac{\varnothing}{\lambda}\right) * t^{n-2}}{(n-2)!} - \cdots \leq \tilde{x}e^{\lambda t} - \tilde{x}(0) \leq \frac{\varnothing}{\lambda^{n-1}}e^{\lambda t} - \frac{\varnothing}{\lambda^{n-1}} + \frac{\left(\left|\frac{d}{dt^{n-2}}\left(\tilde{x}e^{\lambda t}\right)\right|_{t=0} + \frac{\varnothing}{\lambda}\right) * t^{n-2}}{(n-2)!} + \cdots$$

is obtained. Based on the previous similar practice, the term $\tilde{x}(0)$ is added to each side, and once again reminding that $\varnothing$ and λ are positive definite constants and that $\tilde{x}(0) \geq -|\tilde{x}(0)|, \tilde{x}(0) \leq |\tilde{x}(0)|$, if the inequalities, $\frac{\varnothing}{\lambda^{n-1}} \geq -\frac{\varnothing}{\lambda^{n-1}}, \frac{-\varnothing}{\lambda^{n-1}} \leq \frac{\varnothing}{\lambda^{n-1}}$, are used,

$$\frac{-\varnothing}{\lambda^{n-1}}e^{\lambda t} - \frac{\left(\left|\frac{d}{dt^{n-2}}\left(\tilde{x}e^{\lambda t}\right)\right|_{t=0} + \frac{\varnothing}{\lambda}\right) * t^{n-2}}{(n-2)!} - \cdots - \left(|\tilde{x}(0)| + \frac{\varnothing}{\lambda^{n-1}}\right) \leq \tilde{x}e^{\lambda t} \leq \frac{\varnothing}{\lambda^{n-1}}e^{\lambda t} + \frac{\left(\left|\frac{d}{dt^{n-2}}\left(\tilde{x}e^{\lambda t}\right)\right|_{t=0} + \frac{\varnothing}{\lambda}\right) * t^{n-2}}{(n-2)!} + \cdots + \left(|\tilde{x}(0)| + \frac{\varnothing}{\lambda^{n-1}}\right) \tag{55}$$

is written. Also, if (55) is divided into $e^{\lambda t}$ and t is taken to infinity, the following result is obtained:

$$\frac{-\varnothing}{\lambda^{n-1}} - \frac{1}{e^{\lambda t}}\frac{\left(\left|\frac{d}{dt^{n-2}}\left(\tilde{x}e^{\lambda t}\right)\right|_{t=0} + \frac{\varnothing}{\lambda}\right) * t^{n-2}}{(n-2)!} - \cdots - \frac{1}{e^{\lambda t}}\left(|\tilde{x}(0)| + \frac{\varnothing}{\lambda^{n-1}}\right) \leq \tilde{x}(t) \leq \frac{\varnothing}{\lambda^{n-1}} + \frac{1}{e^{\lambda t}}\frac{\left(\left|\frac{d}{dt^{n-2}}\left(\tilde{x}e^{\lambda t}\right)\right|_{t=0} + \frac{\varnothing}{\lambda}\right) * t^{n-2}}{(n-2)!} + \cdots + \frac{1}{e^{\lambda t}}\left(|\tilde{x}(0)| + \frac{\varnothing}{\lambda^{n-1}}\right).$$

From here, it can be easily verified that

$$\frac{-\varnothing}{\lambda^{n-1}} \leq \tilde{x}(t) \leq \frac{\varnothing}{\lambda^{n-1}}. \tag{56}$$

Taking into account the $(n-2)th$ integral of (50),

$$\frac{-\varnothing}{\lambda^{n-2}}e^{\lambda t} - \frac{\left(\left|\frac{d}{dt^{n-2}}\left(\tilde{x}e^{\lambda t}\right)\right|_{t=0} + \frac{\varnothing}{\lambda}\right) * t^{n-3}}{(n-3)!} - \cdots - \left(|\dot{\tilde{x}}(0)| + \frac{\varnothing}{\lambda^{n-2}}\right) \leq \frac{d}{dt}\left(\tilde{x}e^{\lambda t}\right) \leq \frac{\varnothing}{\lambda^{n-2}}e^{\lambda t} + \frac{\left(\left|\frac{d}{dt^{n-2}}\left(\tilde{x}e^{\lambda t}\right)\right|_{t=0} + \frac{\varnothing}{\lambda}\right) * t^{n-3}}{(n-3)!} + \cdots + \left(|\dot{\tilde{x}}(0)| + \frac{\varnothing}{\lambda^{n-2}}\right), \tag{57}$$

and the derivative expression,

$$d\left(\tilde{x}e^{\lambda t}\right)/dt = \dot{\tilde{x}}e^{\lambda t} + \tilde{x}\lambda e^{\lambda t},$$

by having (56)'s bounds accepted to (57) and dividing it back into $e^{\lambda t}$ for $t \to \infty$,

$$\frac{-\varnothing}{\lambda^{n-2}} - (\bullet)\frac{t^{n-3}}{(n-3)!e^{\lambda t}} - \cdots - (\bullet)\frac{1}{e^{\lambda t}} \leq \dot{\tilde{x}}(t) + \tilde{x}(t)\lambda \leq \frac{\varnothing}{\lambda^{n-2}} + (\bullet)\frac{t^{n-3}}{(n-3)!e^{\lambda t}} + \ldots + (\bullet)\frac{1}{e^{\lambda t}},$$

and finally from here,

$$\frac{-\varnothing}{\lambda^{n-2}} \leq \dot{\tilde{x}}(t) + \lambda\tilde{x}(t) \leq \frac{\varnothing}{\lambda^{n-2}} \tag{58}$$

is obtained. However, in order to determine the bounds of (58) based on only $\dot{\tilde{x}}(t)$, the bounds corresponding to the term $\lambda x(t)$ in addition to $\dot{\tilde{x}}(t)$ must be determined exactly. For this, (56) is used and if each side in this inequality is multiplied by λ,

$$\frac{-\varnothing}{\lambda^{n-2}} \leq \lambda\tilde{x}(t) \leq \frac{\varnothing}{\lambda^{n-2}} \tag{59}$$

expression is obtained. Now then, if the effect of $\lambda\tilde{x}(t)$ in the inequality of (58) is substituted by the bound determination ascertained by (59) above, the inequality (59) turns into

$$-2\frac{\varnothing}{\lambda^{n-2}} \leq \dot{\tilde{x}}(t) \leq 2\frac{\varnothing}{\lambda^{n-2}}. \tag{60}$$

Similarly, taking into account the $(n-3)th$ integral of (50),

$$\frac{-\varnothing}{\lambda^{n-3}}e^{\lambda t} - \frac{\left(\left|\frac{d}{dt^{n-3}}\left(\tilde{x}e^{\lambda t}\right)\right|_{t=0} + \frac{\varnothing}{\lambda}\right) * t^{n-4}}{(n-4)!} - \cdots - \left(\left|\ddot{\tilde{x}}(0)\right| + \frac{\varnothing}{\lambda^{n-3}}\right) \leq \frac{d^2}{dt^2}\left(\tilde{x}e^{\lambda t}\right) \leq \frac{\varnothing}{\lambda^{n-3}}e^{\lambda t} + \frac{\left(\left|\frac{d^{n-3}}{dt^{n-3}}\left(\tilde{x}e^{\lambda t}\right)\right|_{t=0} + \frac{\varnothing}{\lambda}\right) * t^{n-4}}{(n-4)!} + \cdots + \left(\left|\ddot{\tilde{x}}(0)\right| + \frac{\varnothing}{\lambda^{n-3}}\right), \tag{61}$$

and the derivative expression,

$$d\left(\dot{\tilde{x}}e^{\lambda t} + \tilde{x}\lambda e^{\lambda t}\right)/dt = \ddot{\tilde{x}}e^{\lambda t} + \lambda e^{\lambda t}\dot{\tilde{x}} + \dot{\tilde{x}}\lambda e^{\lambda t} + \tilde{x}\lambda^2 e^{\lambda t} = \ddot{\tilde{x}}e^{\lambda t} + 2\dot{\tilde{x}}\lambda e^{\lambda t} + \tilde{x}\lambda^2 e^{\lambda t},$$

by imposing the bounds of (56) and (60) on (61) and dividing this expression once again to $e^{\lambda t}$ for $t \to \infty$, the following step is obtained first:

$$\frac{-\varnothing}{\lambda^{n-3}}e^{\lambda t} \leq \ddot{\tilde{x}} + 2\dot{\tilde{x}}\lambda + \tilde{x}\lambda^2 \leq \frac{\varnothing}{\lambda^{n-3}}e^{\lambda t}. \tag{62}$$

Now, the bounds for $\tilde{x}\lambda^2$ and $2\dot{\tilde{x}}\lambda$ are respectively determined with,

$$\frac{-\varnothing}{\lambda^{n-3}} \leq \lambda^2\tilde{x}(t) \leq \frac{\varnothing}{\lambda^{n-3}} \tag{63}$$

by multiplying each side of the inequality of (56) by the term λ^2, and with,

$$-4\frac{\varnothing}{\lambda^{n-3}} \leq 2\dot{\tilde{x}}\lambda \leq 4\frac{\varnothing}{\lambda^{n-3}} \tag{64}$$

by multiplying each side of inequality of (60) by the term 2λ. Once these bounds determined by the inequalities (63) and (64) are imposed on (62), the expression,

$$\frac{-\varnothing}{\lambda^{n-3}} - \frac{\varnothing}{\lambda^{n-3}} - 4\frac{\varnothing}{\lambda^{n-3}} \leq \ddot{\tilde{x}} \leq \frac{\varnothing}{\lambda^{n-3}} + \frac{\varnothing}{\lambda^{n-3}} + 4\frac{\varnothing}{\lambda^{n-3}},$$

and hence in brief, the result,

$$6\frac{\varnothing}{\lambda^{n-3}} \leq \ddot{\tilde{x}} \leq 6\frac{\varnothing}{\lambda^{n-3}} \tag{65}$$

is concluded. As in obtaining (56), (60) and (65), the following general conclusion is reached if the similar procedure is applied sequentially until the bounds of $\tilde{x}^{(n-1)}$ are achieved:

$$-\left(1+\sum_{i=0}^{n-2}\binom{n-1}{i}\zeta_i\right)\varnothing \leq \tilde{x}^{(n-1)} \leq \left(1+\sum_{i=0}^{n-2}\binom{n-2}{i}\zeta_i\right)\varnothing. \tag{66}$$

Here, the coefficients $\zeta_i (i = 0, 1, \cdots, n-2)$ are related to the pre-acquired bounds of each $\tilde{x}^{(i)}$ and are summarized in Theorem 2.

In this way, by examining Eqs. (56), (60), (65), and (66) and, as much as other skipped boundaries, the integrals of (50), the tracking error will be kept within the bounds of $\left|\tilde{x}^{(i)}\right| \leq \zeta_i \lambda^{i-n+1}\varnothing$, $i = 0, 1, \cdots, n-1$, where ζ_i is defined by (47).

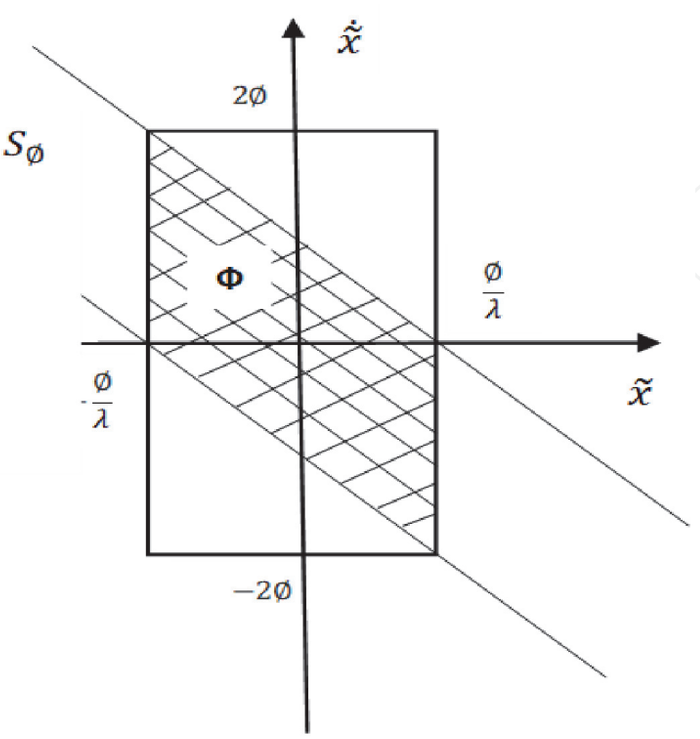

Figure 8.
Convergence region Φ in the case of a second-order system.

Remark 5. It should be noted that an n-dimensionally separated partition defined according to the boundaries mentioned earlier is not entirely within the boundary layer. Considering the attractiveness and invariant properties of $S_{\varnothing}$ proved in Theorem 1, the convergence region can be expressed as the intersection of an n-dimensional separated partition and boundary layer defined in Theorem 2. Thus, the tracking error vector will converge exponentially to a closed region $\Phi = \left\{x \in \boldsymbol{R}^n \middle| |s(\tilde{x})| \leq \varnothing \text{ and } \left|\tilde{x}^{(i)}\right| \leq \zeta_i \lambda^{i-n+1}\varnothing, i = 0, 1, \cdots, n-1\right\}$, where ζ_i is defined by (47).

Figure 8 describes the Φ convergence region defined according to Remark 5 for a second-order ($n = 2$) system.

6. Numerical experimentation and simulation examples

6.1 Position control system by an armature-controlled dc servo motor

6.1.1 Positioning system description

The plant is an armature-controlled dc servo motor, the scheme of which is given in **Figure 9** [19].

In order to derive the state-space mathematical model from the physics of the motor, we first start by writing Kirchoff's voltage equation around the armature current:

$$e_a(t) = i_a(t)R_a + K_b \frac{d\theta_m}{dt}, \tag{67}$$

where $e_a(t)$ is the armature input voltage to the dc amplifier that drives the motor, $i_a(t)$ is the armature current, R_a is the armature resistance, K_b is a constant of proportionality called the back emf constant, or briefly, the armature constant, and θ_m is the angular displacement of the armature.

The torque, $T_m(t)$, delivered by the motor is expressed separately in relation to both the armature current and the load seen by the armature as follows:

$$T_m(t) = K_t i_a(t) = J_m + \frac{d^2\theta_m}{dt^2} + D_m \frac{d\theta_m}{dt}, \tag{68}$$

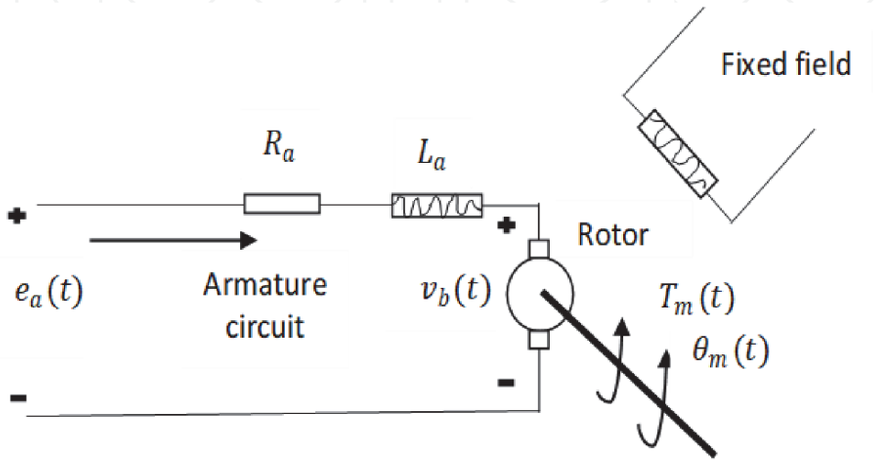

Figure 9.
DC motor schematic diagram.

where J_m and D_m both represent the equivalent inertia and viscous damping seen by the armature, respectively. Solving Eq. (68) for $i_a(t)$ and substituting the result into Eq. (67) yields

$$e_a(t) = \left(\frac{R_a J_m}{K_t}\right)\frac{d^2\theta_m}{dt^2} + \left(\frac{D_m R_a}{K_t} + K_b\right)\frac{d\theta_m}{dt}. \tag{69}$$

Defining the state variables x_1 and x_2 as

$$x_1 = \theta_m, \tag{70}$$

$$x_2 = \frac{d\theta_m}{dt}, \tag{71}$$

and substituting into Eq. (69), we get

$$e_a(t) = \left(\frac{R_a J_m}{K_t}\right)\frac{dx_2}{dt} + \left(\frac{D_m R_a}{K_t} + K_b\right)x_2. \tag{72}$$

Solving for dx_2/dt yields

$$\frac{dx_2}{dt} = \frac{-1}{J_m}\left(D_m + \frac{K_t K_b}{R_a}\right)x_2 + \left(\frac{K_t}{R_a J_m}\right)e_a(t). \tag{73}$$

Using Eqs. (70), (71) and (73), the state equations are written as

$$\frac{dx_1}{dt} = x_2 \tag{74}$$

$$\frac{dx_2}{dt} = \frac{-1}{J_m}\left(D_m + \frac{K_t K_b}{R_a}\right)x_2 + \left(\frac{K_t}{R_a J_m}\right)e_a(t) \tag{75}$$

Hence, in vector-matrix form,

$$\dot{\boldsymbol{x}}(t) = \begin{bmatrix} 0 & 1 \\ 0 & \dfrac{-1}{J_m}\left(D_m + \dfrac{K_t K_b}{R_a}\right) \end{bmatrix}\boldsymbol{x} + \begin{bmatrix} 0 \\ \dfrac{K_t}{R_a J_m} \end{bmatrix}e_a(t).$$

Now, let us consider a position control system and assume a case of varying external disturbance torque to the dc motor. In other words, we assume that a varying external disturbance can enter into the system in the form of varying torque $\tau(t)$ on the shaft of the motor. Therefore, in this derivation, taking account of the external disturbance term which will appear as an extra term in the state equation, we finally describe the state-space representation (a.k.a. the state differential equation) as follows:

$$\dot{\boldsymbol{x}}(t) = \begin{bmatrix} \dot{x}_1(t) \\ \dot{x}_2(t) \end{bmatrix} = \begin{bmatrix} 0 & 1 \\ 0 & -\alpha \end{bmatrix}\begin{bmatrix} x_1(t) \\ x_2(t) \end{bmatrix} + \begin{bmatrix} 0 \\ \kappa \end{bmatrix}e_a(t) - \begin{bmatrix} 0 \\ \gamma \end{bmatrix}\tau(t), \tag{76}$$

where $\boldsymbol{x}(t) = (\, x_1(t) \;\; x_2(t)\,)^T$ has as components the angular position $x_1(t)$ and the angular velocity $x_2(t)$ and where $\alpha \triangleq \frac{1}{J_m}\left(D_m + \frac{K_t K_b}{R_a}\right)$ and $\kappa \triangleq \frac{K_t}{R_a J_m}$, and $\gamma = 1/J$, with J the moment of inertia of all the rotating parts. For the controller variable we choose the angular position:

$$x_1(t) = (1, 0)\boldsymbol{x}(t). \tag{77}$$

The numerical values of motor's parameters have been taken from the case study in [20]:

$$\alpha = 4.6\, s^{-1},$$
$$\kappa = 0.787\, rad/\left(Vs^2\right), \gamma = 0.1\, kg^{-1}m^{-2}.$$

Finally, we try several varying external disturbance torque (Nm) options such as

- $sin\,(at)$, $\gamma sin(at)$, or $msin(at)$, where $a = 3, 4, \cdots$ and m is any appropriate multiplier that is compatible and proportional to the size of the system variables and parameters.

- $sin\,(2\pi t)$, $\gamma sin(2\pi t)$, or $msin(2\pi t)$, where m is defined as one above.

- $sin\,(x_1)$, $\gamma sin(x_1)$, or $msin(x_1)$.

as examples, and we decide that the torque of $\tau(t) = sin(3t)\ Nm$ is the one we choose for the numerical experimentation and simulations as trade-off after we weigh the pros and cons upon several performance tests and considerations. In addition, the simulations given for the DC motor have been run in the form of script code using Matlab [21].

6.1.2 Design of the sliding mode controller for the position control system

Sliding mode surface is defined as:

$$s(t) = ce(t) + \dot{e}(t), \tag{78}$$

where $e(t) = r(t) - x_1(t)$, $\dot{e}(t) = \dot{r}(t) - x_2(t)$, and $r(t)$ is a desired input signal and defined as $r(t) = Asin(2\pi Ft)$in the simulations where A and F are suitably determined, and c is a positive constant. Therefore, once we get a derivative of the expression above, we get the following:

$$\dot{s}(t) = c\dot{e}(t) + \ddot{e}(t) = c\dot{e}(t) + \ddot{r}(t) - \dot{x}_2(t).$$

Taking the second row from Eq. (76) and replacing it with $\dot{x}_2(t)$ above yields:

$$\dot{s}(t) = c\dot{e}(t) + \ddot{r}(t) + \alpha x_2(t) - \kappa e_a(t) + \gamma\tau(t). \tag{79}$$

Next, we obtain the control law $e_a(t)$ by equalizing $\dot{s}(t)$ to zero and then using $\gamma = 1/J$ and $\tau(t) = Ksgn(s(t))$ in Eq. (79) as follows:

$$e_a(t) = \frac{1}{\kappa}[c\dot{e}(t) + \ddot{r}(t) + \alpha x_2(t) + \frac{Ksgn(s(t))}{J}]. \tag{80}$$

Once Eq. (80) is substituted into Eq. (79), we obtain the following:

$$\dot{s}(t) = \frac{\tau(t)}{J} - \frac{Ksgn(s(t))}{J}. \tag{81}$$

where K is a positive constant. Letting $K = max\,(|\tau(t)|) + \eta J$, where $\eta > 0$, and multiplying (81) by $s(t)$ yields:

$$s(t)\dot{s}(t) = \frac{\tau(t)}{J}s(t) - \frac{max\left(|\tau(t)|\right) + \eta J}{J}|s(t)|,$$

Here, the following can always be written:

$$s(t)\dot{s}(t) = \frac{\tau(t)}{J}s(t) - \frac{max\left(|\tau(t)|\right)}{J}|s(t)| - \eta|s(t)| \leq -\eta|s(t)|. \tag{82}$$

Remark 6. It is not difficult to briefly demonstrate the validity of the inequality (82) from a practical point of view: if $s(t)$ is greater than zero (i.e., $s(t) > 0$), then Z term, which we define as $\frac{\tau(t)}{J}s(t) - \frac{max\left(|\tau(t)|\right)}{J}|s(t)|$ from (82), becomes less than zero (i.e., $Z\ term < 0$); because $\frac{max\left(|\tau(t)|\right)}{J}|s(t)| > \frac{\tau(t)}{J}s(t)$. Since the larger term has a negative sign, the difference between the terms will also be negative. As a result, $(some\ negative\ term) - \eta|s(t)| \leq -\eta|s(t)|$ is always valid and correct. If $s(t) < 0$, then $\frac{\tau(t)}{J}s(t) < 0$; in addition, $\frac{-max\left(|\tau(t)|\right)}{J}\underbrace{|s(t)|}_{>0} < 0$, therefore the addition of two negative terms will make the overall addition more negative; hence, $(more\ negative\ term) - \eta|s(t)| \leq -\eta|s(t)|$ which means that the inequality is still valid and in the right direction. Therefore, $\frac{1}{2}\frac{d}{dt}(s^2(t)) \leq -\eta|s(t)|$.

In order to decrease the chattering phenomenon caused by sliding mode control law, saturation function is adapted in this work, and the controller becomes

$$e_a(t) = \frac{1}{\kappa}\left[c\dot{e}(t) + \ddot{r}(t) + \alpha x_2(t) + \frac{K}{J}\overbrace{sat(s(t), \varphi)}^{instead\ of\ sgn(s(t))}\right], \tag{83}$$

where saturation function $sat(s(t), \varphi)$ is defined as,

$$sat(s(t), \varphi) = \begin{bmatrix} \frac{s(t)}{\varphi} |s(t)| \leq \varphi \\ sgn\left(s(t)\right) |s(t)| > \varphi \end{bmatrix}, \tag{84}$$

where φ is a very small positive constant (**Figures 10–18**).

Let us also see how the results will change if PID control is used as an alternative to the SMC. Although, in the comparisons given in the literature, the pros and cons of both strategies are mentioned, it is generally observed that SMC performs better than PID [22–25]. Nevertheless, PID control can still be used as an alternative to SMC. The results given here do not contradict the view that one can use it instead of the other without losing too much performance. In the case where only the PD control strategy is applied, let us state that we need to emphasize the following points for the tracking error performance indicated by **Figure 19**.

We can prefer PD control strategy mostly to advance faster between intermediate points of the entire trajectory, i.e. from waypoint to waypoint at which course is changed for following a reference trajectory in which we have to move end-effector along a predefined path. Speaking of which, the end-effector is crucial for the entire trajectory tracking problem in catching up a desired position within shortest time. In other words, accuracy is highly desirable for the end-effector to be positioned accurately under unknown disturbances and payload variations. Basically, the desired position is a function of time and continuously changes with respect to time. Therefore, conventional PD control strategy does not always exhibit good accuracy and robustness properties for trajectory tracking problem. However, we can still

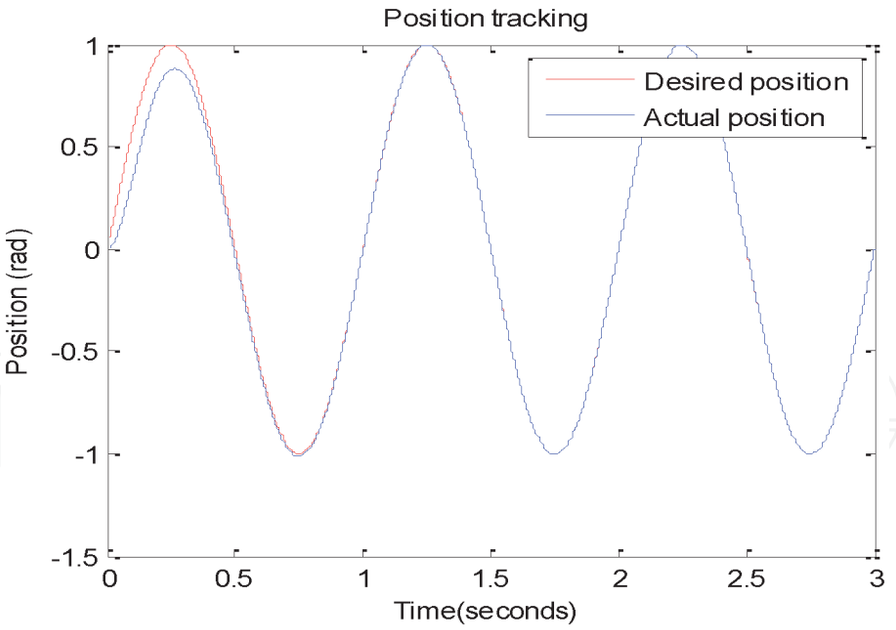

Figure 10.
Position tracking under SMC of the position control system.

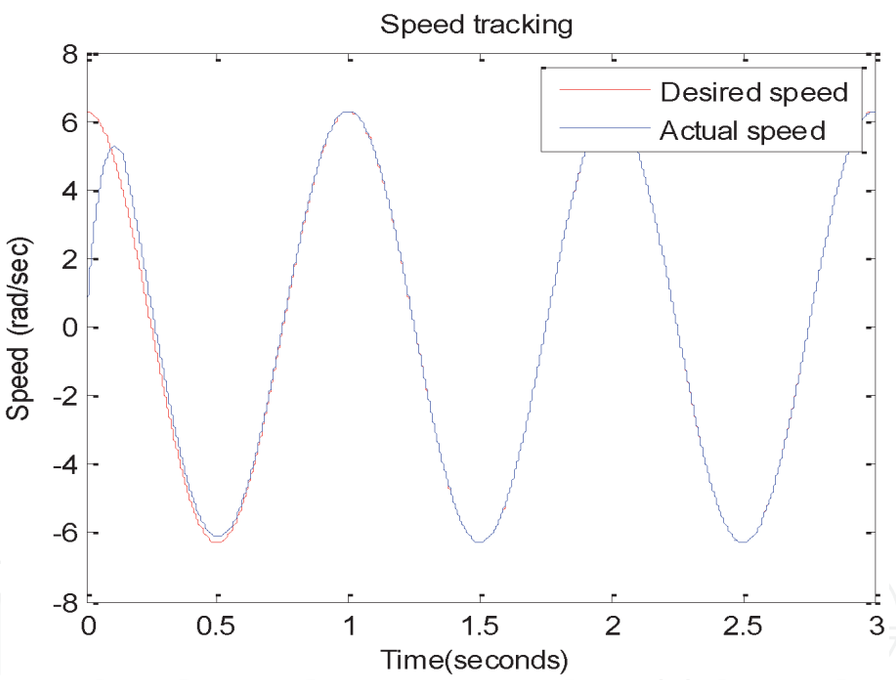

Figure 11.
Speed tracking under SMC of the position control system.

choose the PD control strategy because of the advantages it offers [26]. We should emphasize that the errors between the actual points and the waypoints, each of which can also be viewed as intermediate setpoints, do not necessarily have to be eliminated completely. As a result, we have decided to use the PD control because of the advantages it offers and to move faster between the waypoints by tolerating or neglecting the steady-state error computations that would bring extra computational burden (**Figures 20–22**).

6.2 Modeling and simulation of A two-link (2-DOF) planar robot manipulator

A manipulator consists of an open kinematic chain of rigid links. Power is supplied to each degree of freedom of the manipulator by independent torques. The

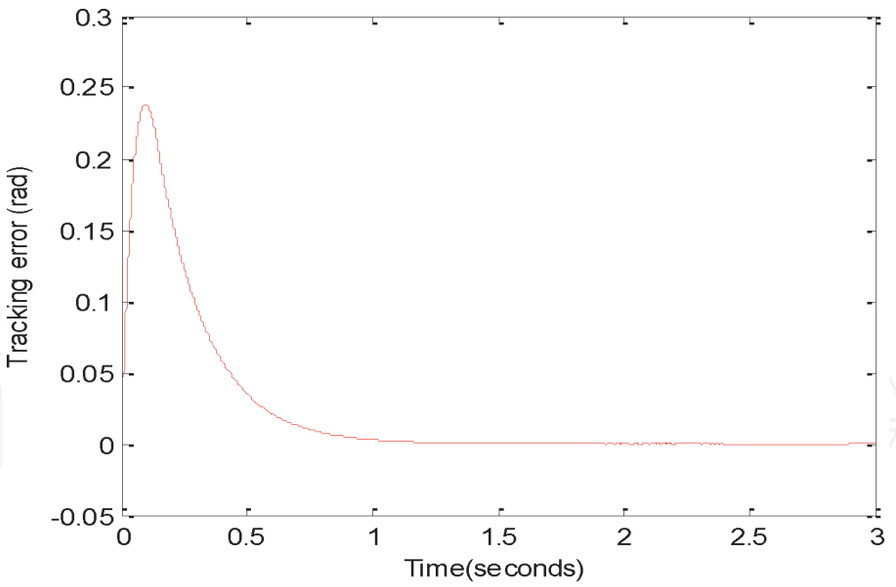

Figure 12.
Tracking error under SMC of the position control system.

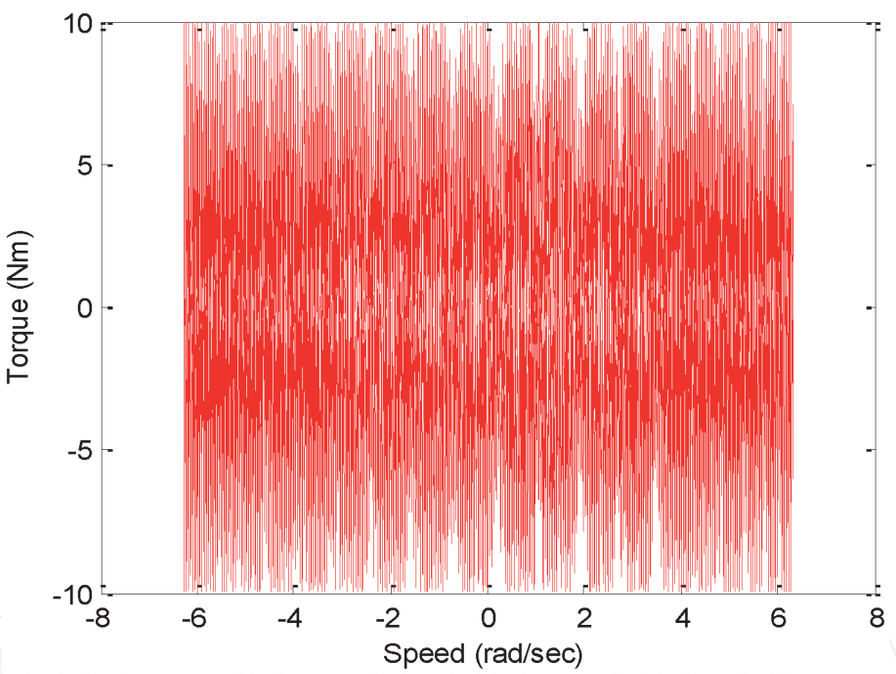

Figure 13.
Torque vs. speed curve under SMC of the position control system.

dynamical equations of motion of an n-link (i.e., n-degree-of-freedom) robot manipulator using the Lagrangian formulation has already been described in Section 3 by the Eq. (8). The robot model there is characterized by the following structural properties which are important for our sliding mode controller design of the tracking problem [27]:

Property 1. *A vector $\boldsymbol{\alpha} \in \boldsymbol{R}^m$ with components that depend on manipulator parameters (masses, moments of inertia, etc.) exists, such that*

$$\boldsymbol{M}(\boldsymbol{q})\dot{\boldsymbol{v}} + \boldsymbol{C}(\boldsymbol{q}, \dot{\boldsymbol{q}})\boldsymbol{v} + \boldsymbol{G}(\boldsymbol{q}) = \boldsymbol{\Phi}(\boldsymbol{q}, \dot{\boldsymbol{q}}, \boldsymbol{v}, \dot{\boldsymbol{v}})\boldsymbol{\alpha}, \tag{85}$$

where $\boldsymbol{\Phi} \in \boldsymbol{R}^{nxm}$ is called the regressor, $\boldsymbol{v} \in \boldsymbol{R}^n$ is a vector of smooth functions. This property implies that the dynamic equation can be linearized according to a specially selected manipulator parameter set, hence constituting the basis for the linear parameterization approach.

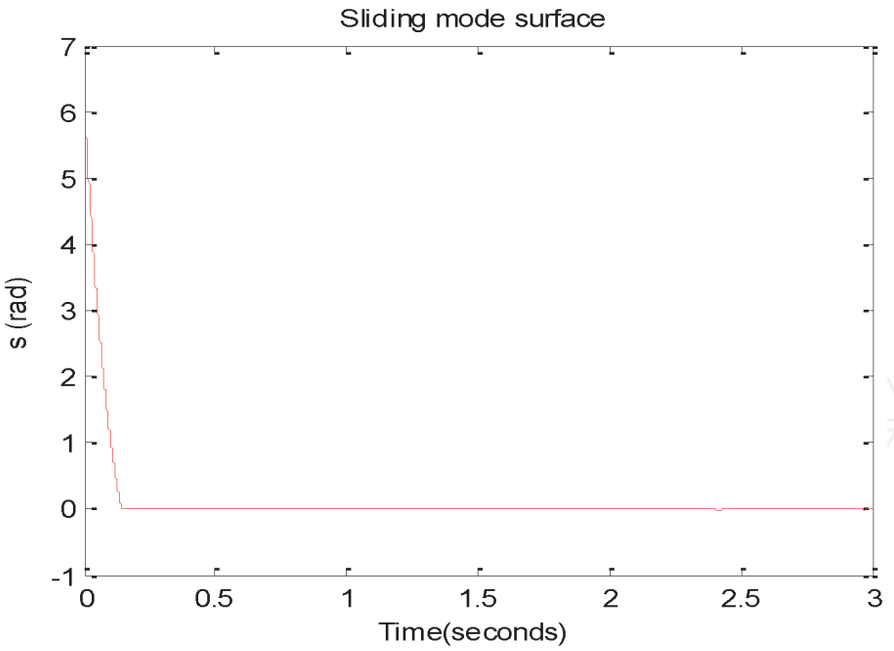

Figure 14.
Sliding mode surface under SMC of the position control system.

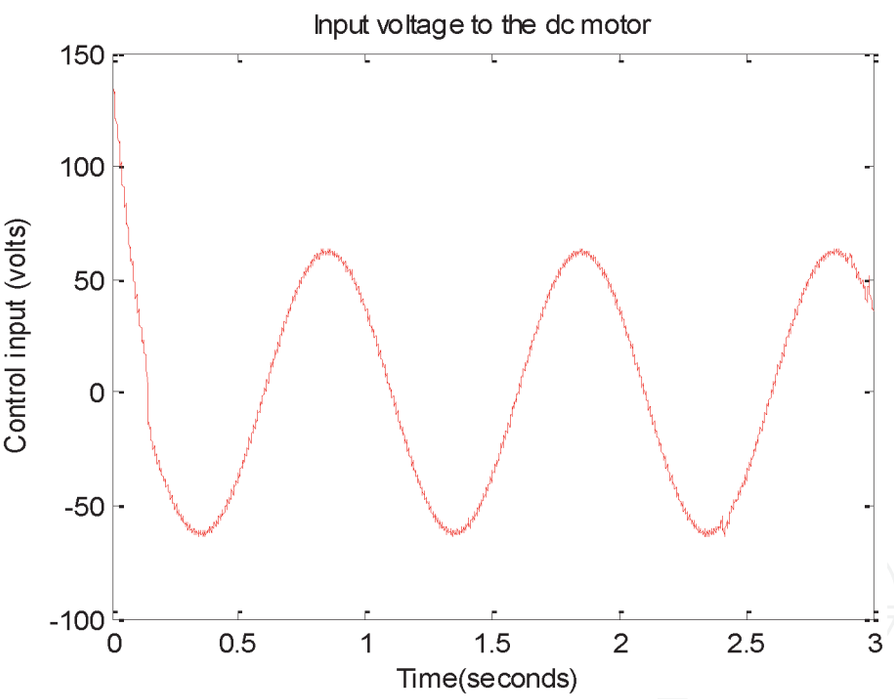

Figure 15.
Control input under SMC of the position control system.

Property 2. *Both* $\boldsymbol{M}(\boldsymbol{q})$ *and* $\boldsymbol{C}(\boldsymbol{q},\dot{\boldsymbol{q}})$ *in Eq. (8), using a properly defined matrix* $\boldsymbol{C}(\boldsymbol{q},\dot{\boldsymbol{q}})$*, satisfy*

$$\boldsymbol{x}^T(\dot{\boldsymbol{M}}-2\boldsymbol{C})\boldsymbol{x}=0,\quad \forall \boldsymbol{x}\in\boldsymbol{R}^n \tag{86}$$

with $\boldsymbol{x}^T$ *the transposition of* $\boldsymbol{x}$*. That is,* $(\dot{\boldsymbol{M}}-2\boldsymbol{C})$ *is a skew-symmetric matrix. Property 2 simply states that the so-called fictitious forces, defined by* $\boldsymbol{C}(\boldsymbol{q},\dot{\boldsymbol{q}})\dot{\boldsymbol{q}}$*, do not work on the system.*

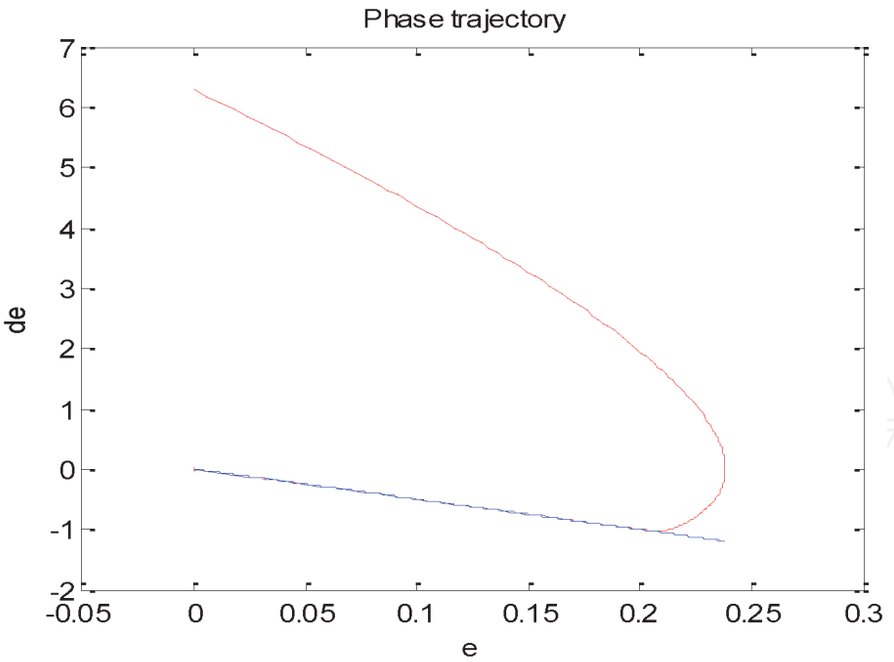

Figure 16.
Phase trajectory under SMC of the position control system.

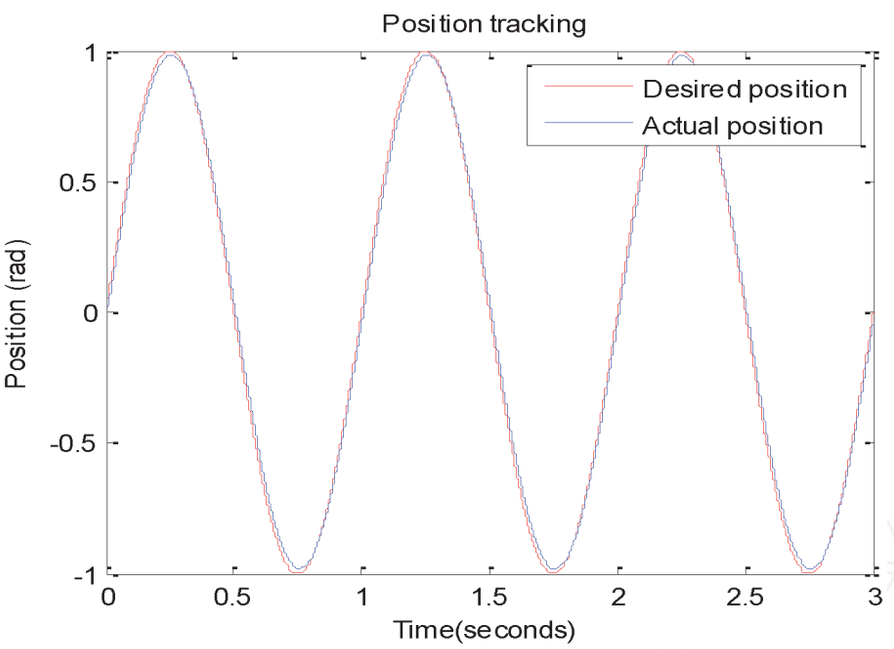

Figure 17.
Position tracking under PD control of the position control system.

The model given in **Figure 23** is known as a two-Link (2-DOF) planar robot, as it corresponds to the two-dimensional special case, where $n = 2$ is taken in the n-link robot manipulator [27].

The dynamic model chosen for the simulations is given by

$$\boldsymbol{M}(\boldsymbol{\theta})\ddot{\boldsymbol{\theta}}_r + \boldsymbol{F}(\boldsymbol{\theta}, \dot{\boldsymbol{\theta}}_r)\dot{\boldsymbol{\theta}}_r + \boldsymbol{G}(\boldsymbol{\theta}) = \boldsymbol{\tau},$$

and the dynamic equation is given by

$$\begin{bmatrix} M_{11} & M_{12} \\ M_{12} & M_{22} \end{bmatrix} \begin{bmatrix} \ddot{\theta}_1 \\ \ddot{\theta}_2 \end{bmatrix} + \begin{bmatrix} -F_{12}\dot{\theta}_2 & -F_{12}(\dot{\theta}_1 + \dot{\theta}_2) \\ F_{12}\dot{\theta}_1 & 0 \end{bmatrix} \begin{bmatrix} \dot{\theta}_1 \\ \dot{\theta}_2 \end{bmatrix} + \begin{bmatrix} G_1 g \\ G_2 g \end{bmatrix} = \begin{bmatrix} u_1 \\ u_2 \end{bmatrix},$$

where

$$M_{11} = (m_1 + m_2)r_1^2 + m_2 r_2^2 + 2m_2 r_1 r_2 \cos(\theta_2)$$

$$M_{12} = m_2 r_2^2 + m_2 r_1 r_2 \cos(\theta_2)$$

$$M_{22} = m_2 r_2^2$$

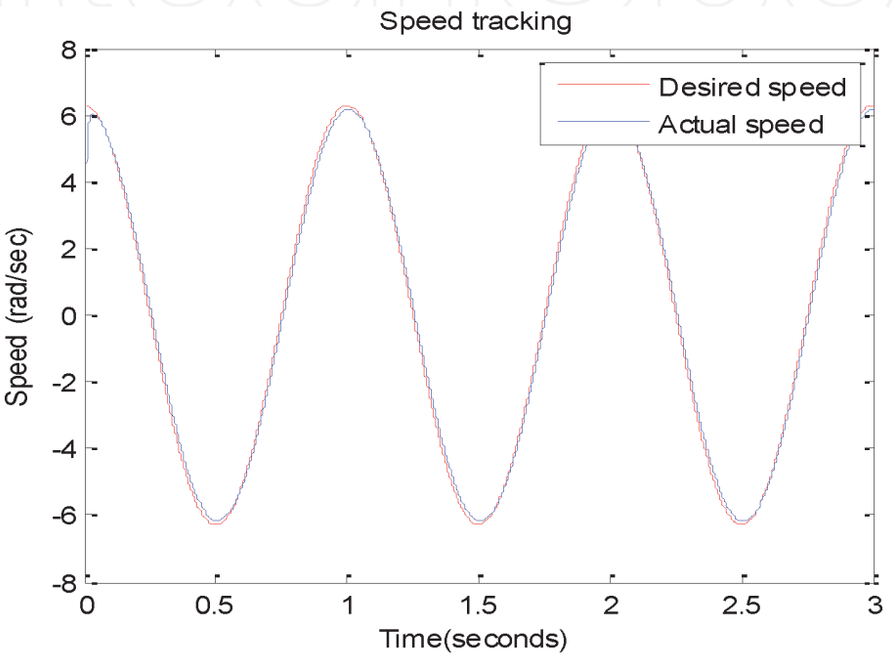

Figure 18.
Speed tracking under PD control of the position control system.

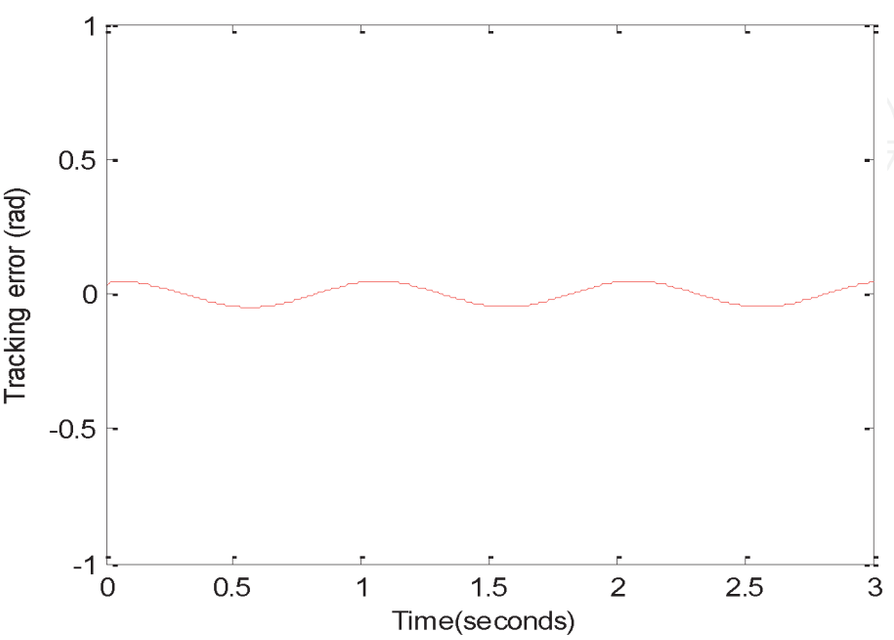

Figure 19.
Tracking error under PD control of the position control system.

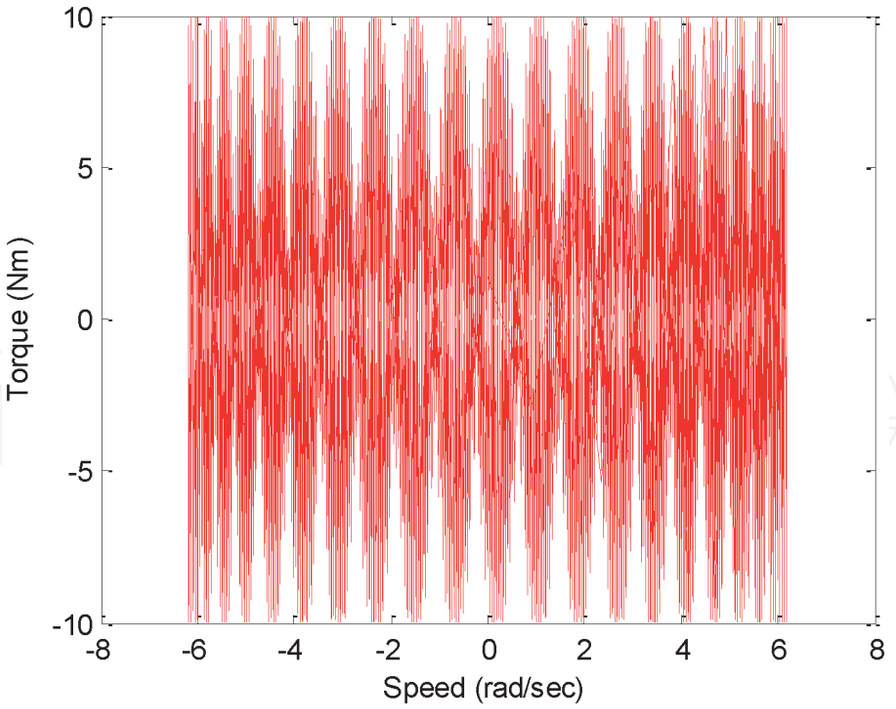

Figure 20.
Torque vs. speed curve under PD control of the position control system.

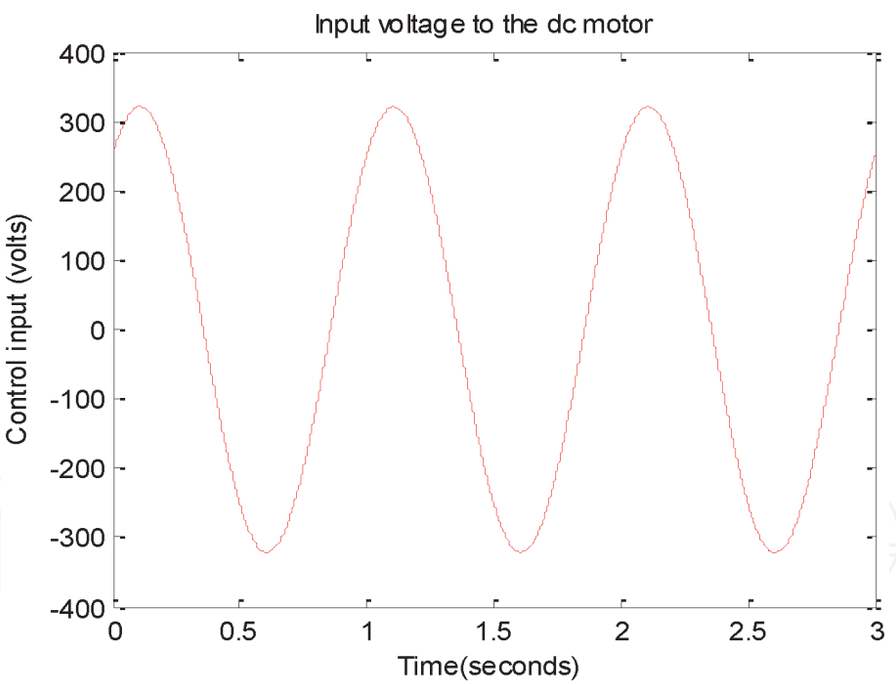

Figure 21.
Control input under PD control of the position control system.

$$F_{12} = m_2 r_1 r_2 \sin(\theta_2)$$

$$G_1 = (m_1 + m_2) r_1 \cos(\theta_2) + m_2 r_2 \cos(\theta_1 + \theta_2)$$

$$G_2 = m_2 r_2 \cos(\theta_1 + \theta_2)$$

6.2.1 No boundary layer

- The desired joint trajectory for each joint (i) is given by [27, 28] as:

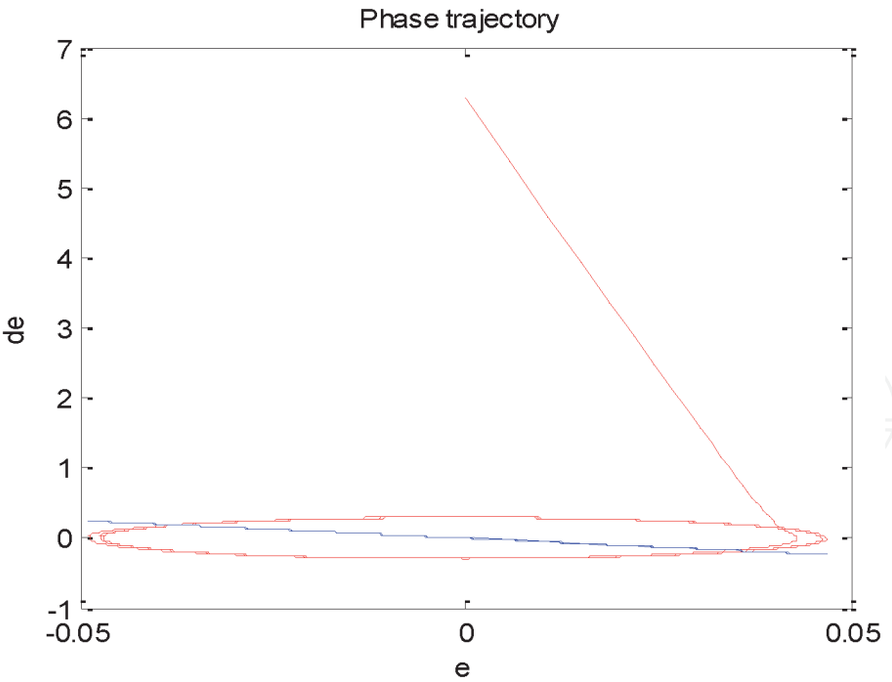

Figure 22.
Phase trajectory under PD control of the position control system.

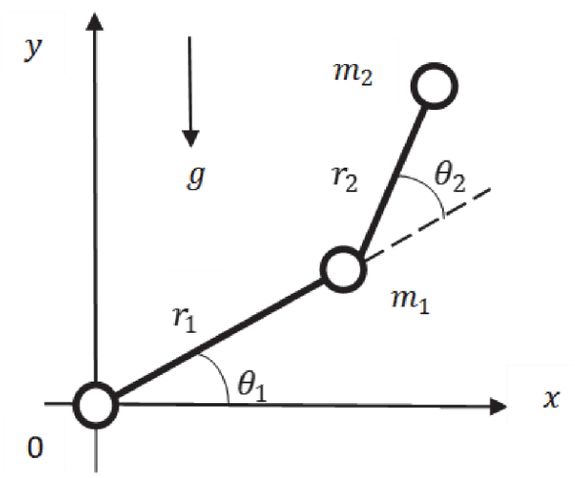

Figure 23.
A two-link robot manipulator model.

$$\theta_d(t) = -90^o + 52.5(1 - \cos(1.26t))$$

- Initial conditions:

$$\theta_1(0) = -45° \text{ and } \theta_2(0) = -30°.$$

- The parameter values used are selected as in [27, 28]:

$$m_1 = 0.5 \text{ kg}, m_2 = 0.5 \text{ kg}$$
$$r_1 = 1.0 \text{ m}, r_2 = 0.8 \text{ m}$$

- Matlab-Simulink implementation options used in the simulations (**Figures 24–31**) as in [28]:

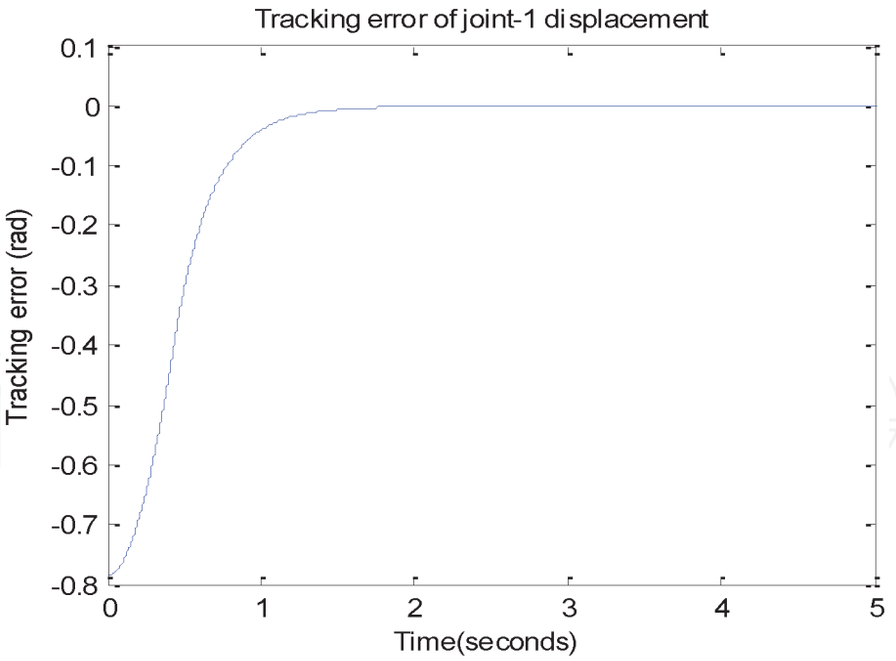

Figure 24.
Tracking error of Joint 1 displacement under SMC of the robot manipulator.

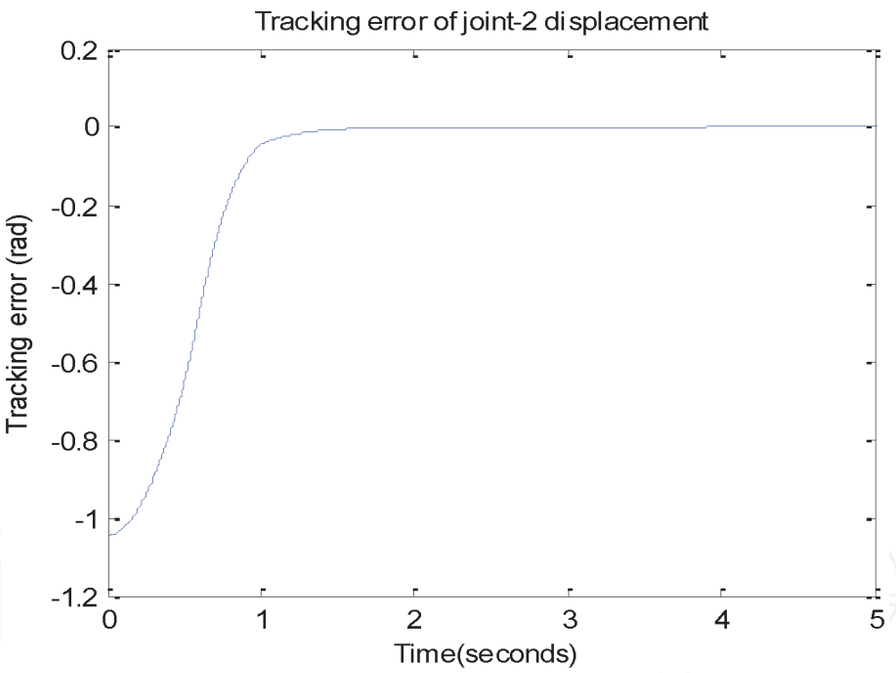

Figure 25.
Tracking error of Joint 2 displacement under SMC of the robot manipulator.

$$\text{Sampling time } T_s = 1\,\text{kHz}, \text{fixed} - \text{step}, \text{ode5}$$

- Joint 1: $K = 14$, $\lambda = 4$, $\phi = 0$.
- Joint 2: $K = 8$, $\lambda = 4$, $\phi = 0$.

6.2.2 Introducing boundary layer

The same parameters and initial conditions for the simulations have been chosen as in Section 6.2.1 except for the following ones which include the boundary layer thickness in particular:

- Joint 1: $K = 14$, $\lambda = 4$, $\phi = 0.02$.
- Joint 2: $K = 8$, $\lambda = 4$, $\phi = 0.02$.

Please note that due to the space constraint, we will be able to give only the figures whose effect is clearly observed, not eight figures as given in Section 6.2.1 (**Figures 32–34**).

For tracking a desired trajectory by two-link rigid planar robotic manipulator, PID control strategy will not work well under unknown disturbances and payload changes, and hence will not be represented here. In addition, the values of control input will get

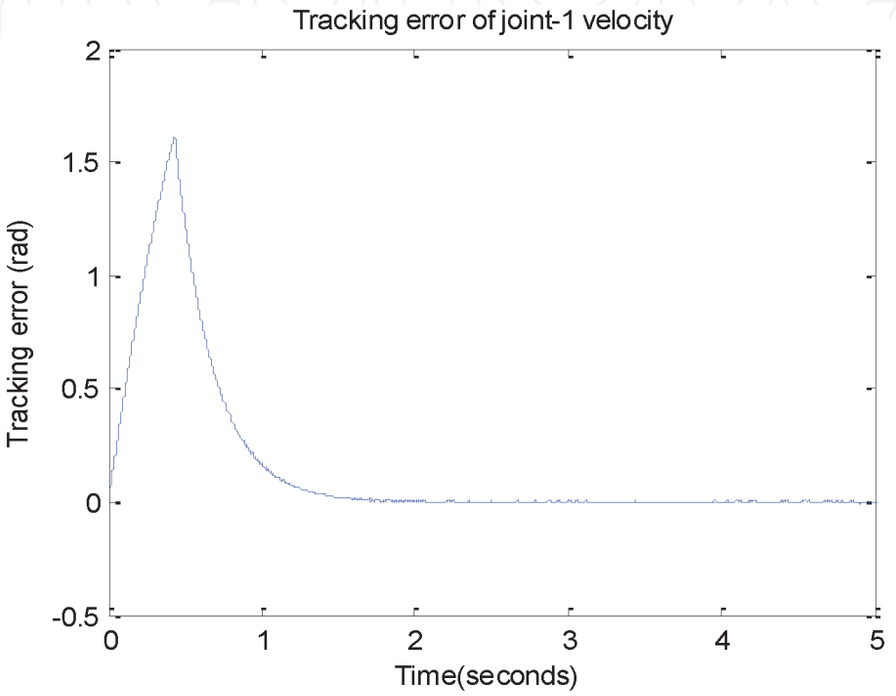

Figure 26.
Tracking error of Joint 1 velocity under SMC of the robot manipulator.

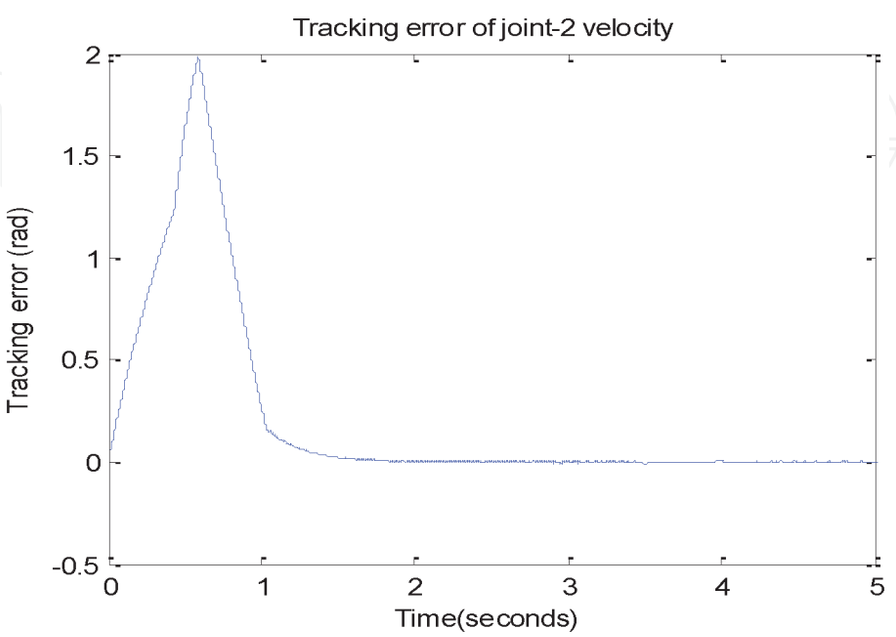

Figure 27.
Tracking error of Joint 2 velocity under SMC of the robot manipulator.

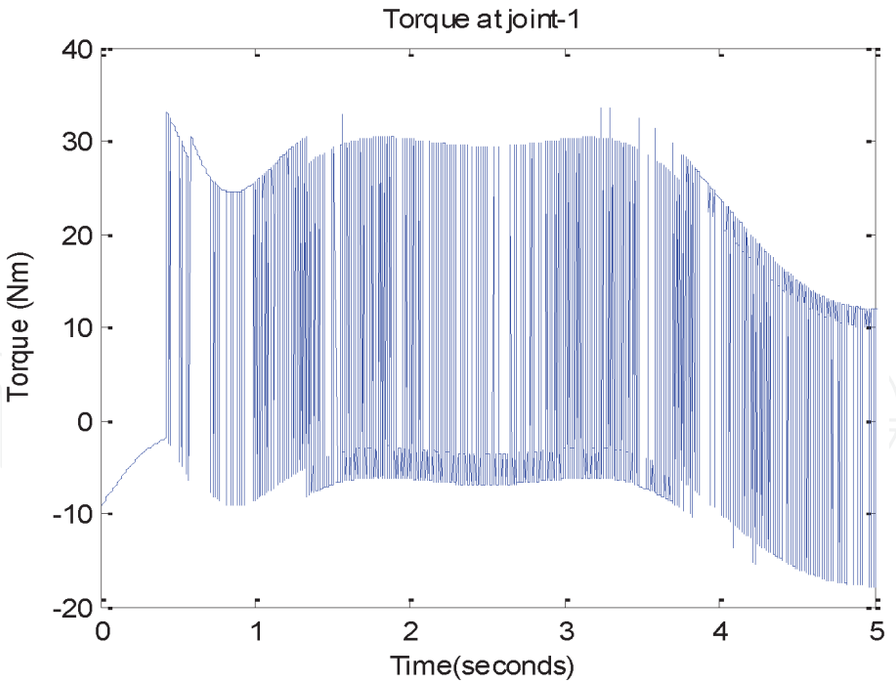

Figure 28.
Torque at Joint 1 under SMC of the robot manipulator.

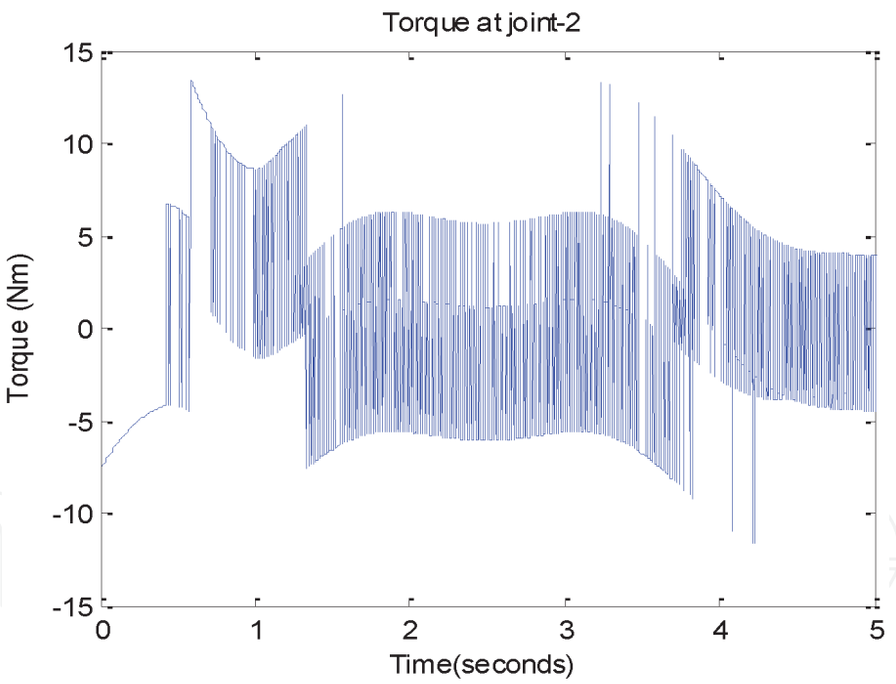

Figure 29.
Torque at Joint 2 under SMC of the robot manipulator.

higher as in the case of DC motor position control and that would complicate the realization of such high gains through the proper actuators. On the other hand, SMC provides robustness against parameter uncertainties and unmodeled disturbances so long as the observed undesirable chattering effect is overcome through some modifications by simply replacing nonlinear signum function with nonlinear saturation function and introducing boundary layer thickness in there as explained in earlier sections. In order to realize this, the boundary layer has been introduced for the first time in Section 6.2.2 simulations, and consequently, no switching or chattering effect has been observed as can be verified by the phase portrait in **Figure 34**.

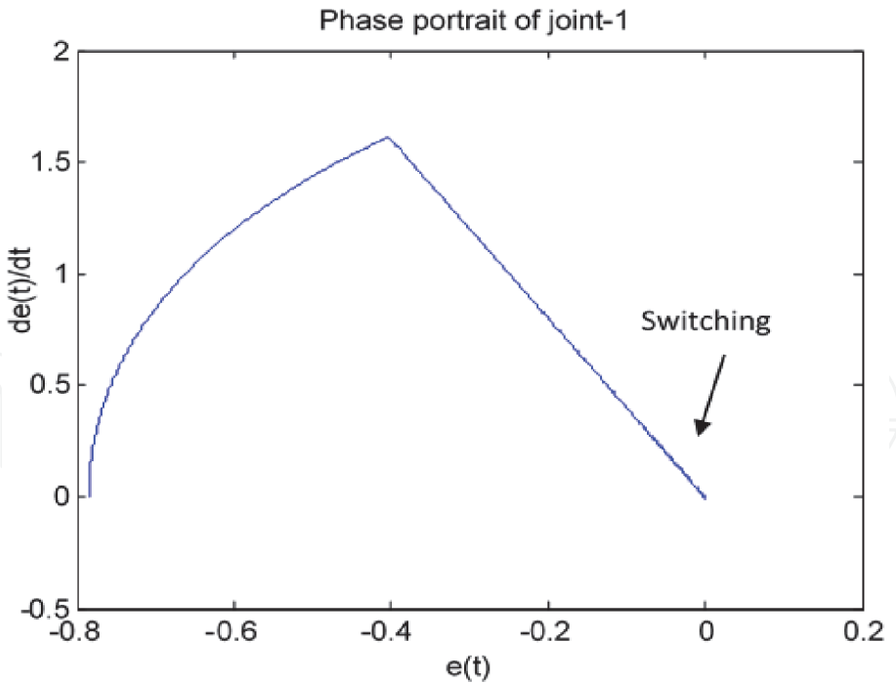

Figure 30.
Phase portrait of Joint 1 under SMC of the robot manipulator.

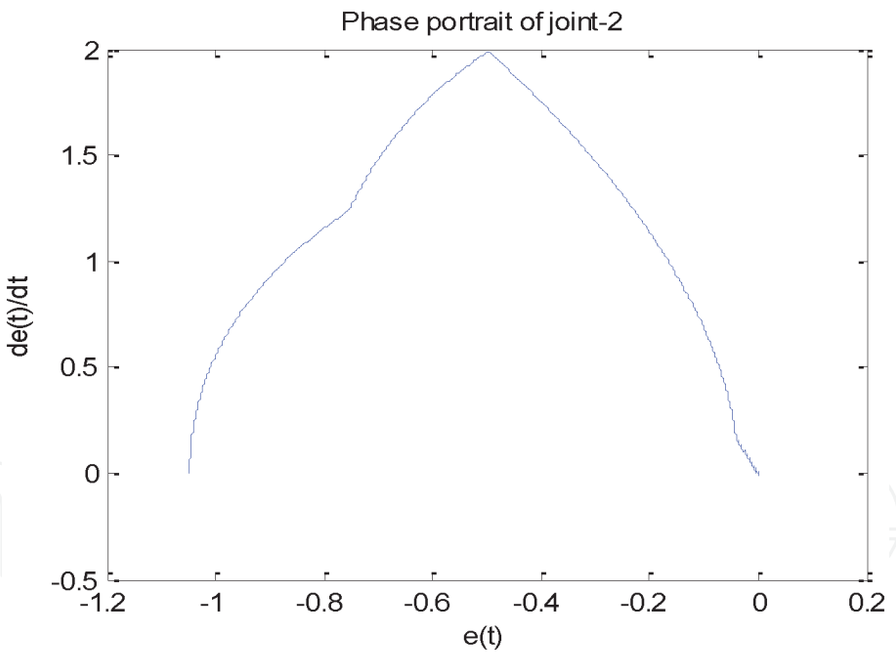

Figure 31.
Phase portrait of Joint 2 under SMC of the robot manipulator.

Later, the robustness of the SMC will be analyzed by adding an extra mass of 0.5 kg to Joint 2, and we have not observed any performance degradation of the trajectory to be maintained in the sliding surface. Therefore, the controller is said to be robust enough. However, it is expected that switching will reappear to maintain the trajectory in the sliding surface.

As a rule of thumb, It is possible to do tracking with more load by reducing the boundary layer to allow more switching to occur. Now, we reduce the boundary layer thickness from 0.02 to 0.005 and add the extra mass to Joint 2 by 0.75 kg to a final of 1.25 kg and we can still observe that SMC will be able to do the tracking by

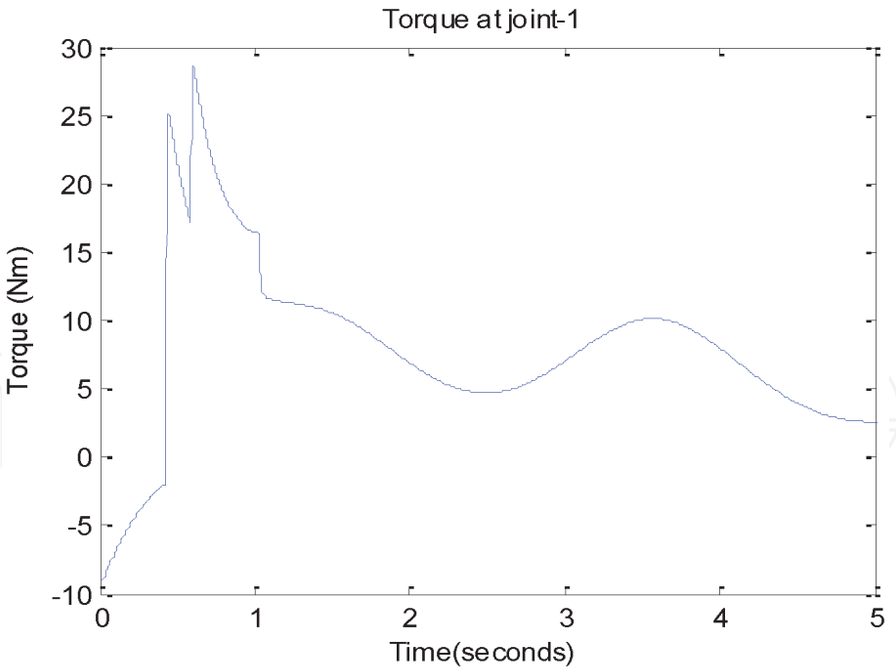

Figure 32.
Torque at of Joint 1 under SMC with a boundary layer.

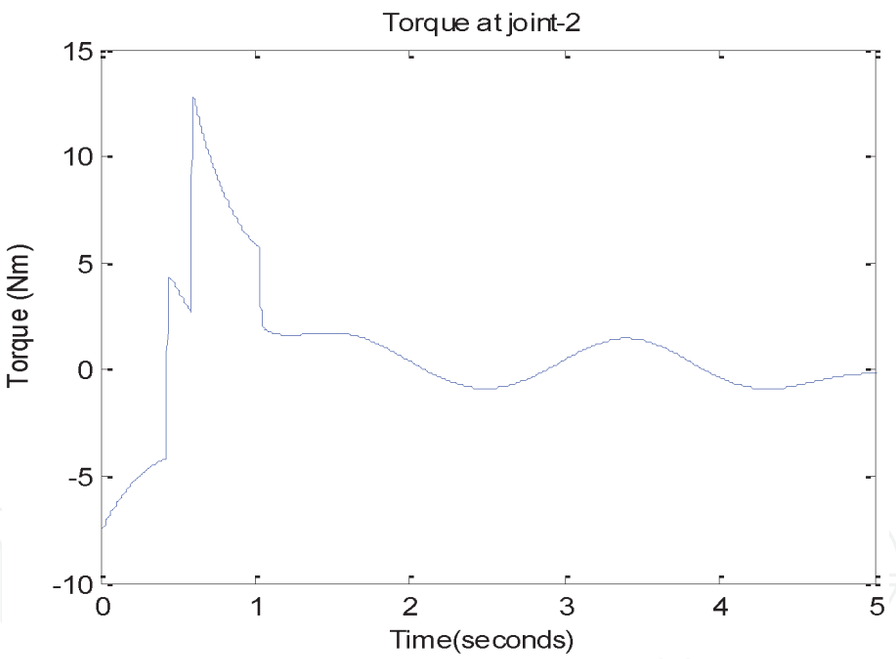

Figure 33.
Torque at of Joint 2 under SMC with a boundary layer.

observing the reemerged chattering effect as can be seen in the following simulations (**Figure 35**):

- Joint 1: $K = 14$, $\lambda = 4$, $\phi = 0.005$.
- Joint 2: $K = 8$, $\lambda = 4$, $\phi = 0.005$.
- $m_1 = 0.5$ kg, $m_2 = 1.25$ kg (an extra mass of 0.75 kg was added to Joint 2).
- The rest of the parameters and the IC's were kept the same as before.

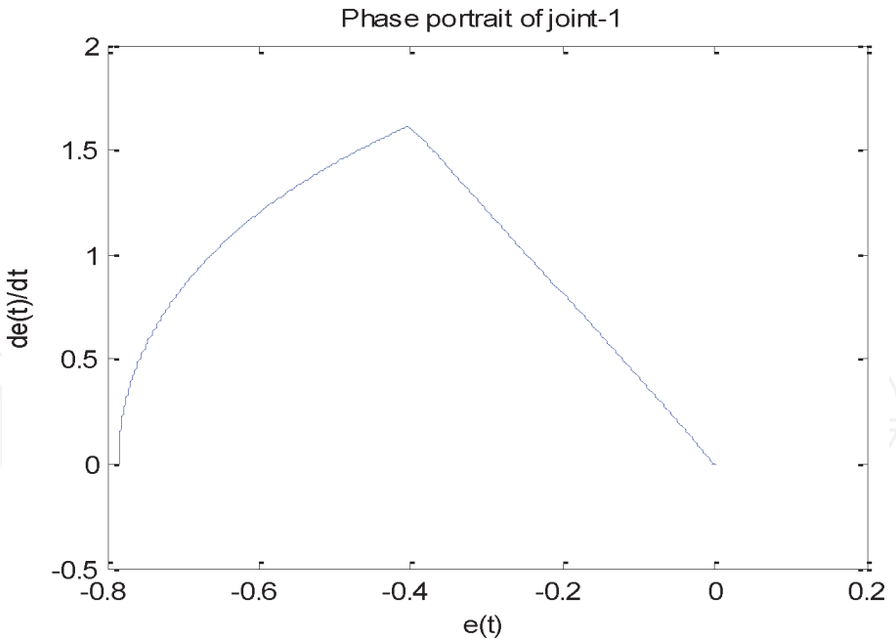

Figure 34.
Phase portrait of Joint 1 under SMC with a boundary layer.

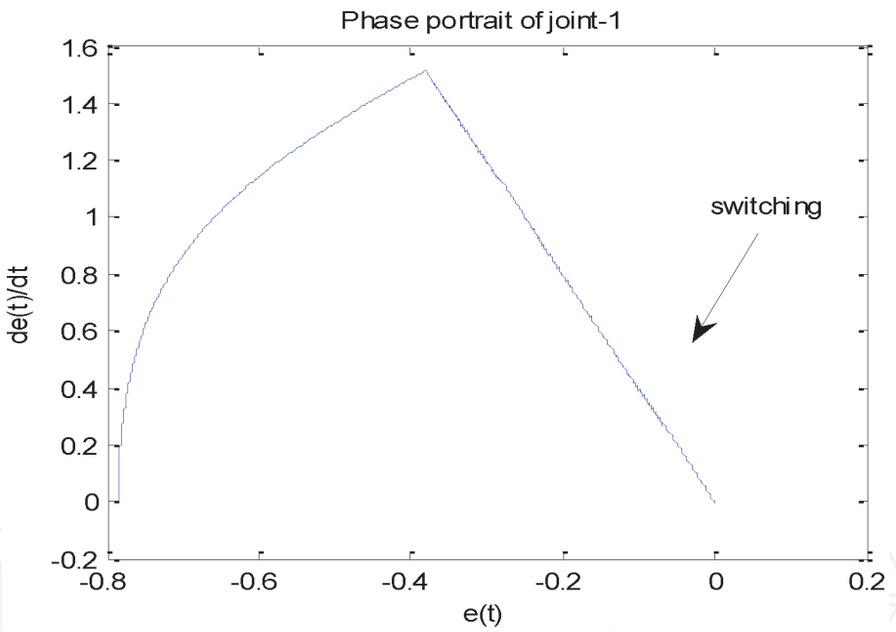

Figure 35.
Phase portrait of Joint 1 under SMC with a robustness test including more load.

7. Conclusions

In this study, a sliding mode control scheme with a bounded region and its convergence analysis are explained to the finest detail. In particular, it can easily be said that the work done here is a field study that specifically gives the relevant subject with such meticulous detail. It is our claim that this study has a guiding identity for the researchers who are interested in this control method or want to present it with the intelligent and modern control methodologies with its understandability and clarity targeted here. In this regard, the design of SMC including its finite-time convergence is handled by using Lyapunov's direct method. The tracking error vector converges exponentially to the bounded region once in the

boundary layer as proven analytically. Two examples were used for simulation studies to demonstrate the feasibility and effectiveness of the proposed control problems, i.e., the position control of a dc motor subject to a varying external disturbance, and a two-link robot manipulator. Simulations show that a fast convergence rate, and hence quick response, the ability to reject the varying external disturbances, and the robustness against the model uncertainty assumed to be unbounded and fast-varying have all achieved its purpose entirely. Chattering is eliminated by using the boundary layer whose attractiveness and invariance properties of the boundary layer were also introduced. This study also examines the advantages of SMC and PID comparably. Although, in the comparisons given in the literature, the pros and cons of both strategies are mentioned, it is generally observed that SMC performs better than PID. Nevertheless, PID control can still be used as an alternative to SMC. When the PID control strategy does not work well under unknown disturbances and payload changes, SMC provides robustness against parameter uncertainties and unmodeled disturbances so long as the observed undesirable chattering effect is overcome through some modifications as described in the text. Robustness analysis has been performed and successfully applied to the two-link rigid planar robotic manipulator. We have not observed any performance degradation of the trajectory to be maintained in the sliding surface. The results given here do not contradict the view that one can use it instead of the other without losing too much performance. Finally, a two-step simulation has been carried out, testing all the features mentioned above, and the results have confirmed the success of the presented approach. However, it is meaningful and challenging to develop new SMC theories and methods for nonlinear systems due to its broad application potentials in today's world.

Conflict of interest

The authors declare no conflict of interest.

Author details

İhsan Ömür Bucak
Istanbul Rumeli University, Istanbul, Turkey

*Address all correspondence to: iomur.bucak@rumeli.edu.tr

References

[1] Slotine J, Li W. Applied Nonlinear Control. New Jersey: Prentice-Hall; 1991. p. 461. ISBN: 0-13-040890-5

[2] Shafiei SE. Sliding mode control of robot manipulators via intelligent approaches. In: Shafiei SE, editor. Advanced Strategies for Robot Manipulators. Rijeka: IntechOpen; 2010. pp. 135-172. DOI: 10.5772/10193

[3] Yu X, Kaynak O. Sliding-mode control with soft computing: A survey. IEEE Transactions on Industrial Electronics. 2009;**56**(9):3275-3285. DOI: 10.1109/TIE.2009.2027531

[4] Utkin VI. Variable structure systems with sliding modes. IEEE Transactions on Automatic Control. 1977;**22**(2): 212-222. DOI: 10.1109/TAC.1977.1101446

[5] Tannuri EA, Agostinho AC, Morishita HM, Moratelli L. Dynamic partitioning systems: An experimental analysis of sliding mode control. Control Engineering Practice. 2010;**18**(10): 1121-1132. DOI: 10.1016/j.conengprac.2010.06.007

[6] Young KD, Utkin VI, Ozguner U. A control engineer's guide to sliding mode control. IEEE Transactions on Control Systems Technology. 1999;**7**(3):328-342. DOI: 10.1109/87.761053

[7] Köse E, Kızmaz H, Abacı K, Aksoy S. Control of SVC based on the sliding mode control method. Turkish Journal of Electrical Engineering and Computer Sciences. 2014;**22**:605-619. DOI: 10.3906/elk-1209-8

[8] Bessa WM, Paulo AS, Salvi MA. Sliding mode control with adaptive fuzzy dead-zone compensation for uncertain chaotic systems. Nonlinear Dynamics. 2012;**70**:1989-2001. DOI: 10.1007/s11071-012-0591-z

[9] Chang E. Study and application of intelligent sliding mode control for voltage source inverters. Energies. 2018; **11**(10):14. Article ID 2544. DOI: 10.3390/en11102544

[10] Sun XQ, Cai YF, Yuan CC, Wang SH, Chen L. Fuzzy sliding mode control for the vehicle height and leveling adjustment system of an electronic air suspension. Chinese Journal of Mechanical Engineering. 2018;**31**:13. Article ID 25. DOI: 10.1186/s10033-018-0223-8

[11] Sharkawy AB, Salman SA. An adaptive fuzzy sliding mode control scheme for robotic systems. Intelligent Control and Automation. 2011;**2**(4): 299-309. DOI: 10.4236/ica.2011.24035

[12] Koubaa Y, Boukattaya M, Damak T. Intelligent control for nonholonomic mobile robot including actuator dynamics. In: Proceedings of the 15th International Multi-Conference on Systems, Signals & Devices (SSD); 19–22 March 2018; Hammamet. Tunisia: IEEE; 2018. pp. 1012-1016

[13] Jiang B, Gao C, Kao Y, Liu Z. Sliding mode control of Markovian jump systems with incomplete information on time-varying delays and transition rates. Applied Mathematics and Computation. 2016;**290**(C):66-79. DOI: 10.1016/j.amc.2016.05.038

[14] Leu VQ, Choi HH, Jung JW. LMI-based sliding mode speed tracking control design for surface-mounted permanent magnet synchronous motors. Journal of Electrical Engineering and Technology. 2012;**7**(4):513-523. DOI: 10.5370/JEET.2012.7.4.513

[15] Huynh VV, Tsai YW, Duc PV. Adaptive output feedback sliding mode control for complex interconnected time-delay systems. Mathematical

Problems in Engineering. 2015;**2015**:15. Article ID 239584. DOI: 10.1155/2015/239584

[16] Fallaha CJ, Saad M, Kanaan HY, A-Haddad K. Sliding-mode robot control with exponential reaching law. IEEE Transactions on Industrial Electronics. 2011;**58**(2):600-610. DOI: 10.1109/TIE.2010.2045995

[17] Zhang B, Yang X, Zhao D, Spurgeon SK, Yan X. Sliding mode control for nonlinear manipulator systems. IFAC-PapersOnLine. 2017; **50**(1):5127-5132. DOI: 10.1016/j.ifacol.2017.08.781

[18] Moldoveanu F. Sliding mode controller design for robot manipulators. Bulletin of the Transilvania University of Brasov, Series I: Engineering Sciences. 2014; **7**(2):97-104

[19] Nise NS. Control Systems Engineering. 7th ed. New Jersey: Wiley; 2015. p. 944. ISBN: 978-1-118-17051-9

[20] Kwakernaak H, Sivan R. Linear Optimal Control Systems. New York: Wiley; 1972. p. 595. ISBN: 0-471-51110-2

[21] The MathWorks Inc. MATLAB Version R2013a. Natick, Massachusetts: The MathWorks Inc; 2013

[22] Nasir ANK, Ismail RMTR, Ahmad MA. Performance comparison between sliding mode control (SMC) and PD-PID controllers for a nonlinear inverted pendulum system. International Journal of Computer, Electrical, Automation, Control and Information Engineering. 2010;**4**(10): 1508-1513. Available from: scholar.waset.org/1999.4/1558

[23] Castillo-Zamora JJ, Camarillo-GóMez KA, PéRez-Soto GI, RodríGuez-ReséNdiz J. Comparison of PD, PID and sliding-mode position controllers for V–tail quadcopter stability. IEEE Access. 2018;**6**:38086-38096. DOI: 10.1109/ACCESS.2018.2851223

[24] Yousef AM. Experimental set up verification of servo DC motor position control based on integral sliding mode approach. WSEAS Transactions on Systems and Control. 2012;**7**(3):87-96. E-ISSN: 2224-2856

[25] Rafferty KJ, McGookin EW. A comparison of PID and sliding mode controllers for a remotely operated helicopter. In: Proceedings of the 12th International Conference on Control Automation Robotics & Vision (ICARCV); 5–7 Dec. 2012; Guangzhou, China: IEEE; 2013. pp. 984–989

[26] Xu J, Qiao L. Robust adaptive PID control of robot manipulator with bounded disturbances. Mathematical Problems in Engineering. 2013;**2013**:13. Article ID 535437. DOI: 10.1155/2013/535437

[27] Su CY, Leung TY. A sliding mode control with bound estimation for robot manipulators. IEEE Transactions on Robotics and Automation. 1993;**9**: 208-213. DOI: 10.1109/70.238284

[28] A. Manurung, A Sliding Mode Control for Robot Manipulator [Internet]. 2010. Available from: http://sites.google.com/site/auraliusproject/a-sliding-mode-control-for-robot-manipulator [Accessed: 09 July 2019]